The dyke porphyries in Kiirunavaara - geology, geochemistry, mineralogy, and age

Joachim Pihl 38006-299-2013

joachim.pihl(a)abo.fi

Master's thesis in geology

Supervisors: Ulf B. Andersson and Olav Eklund

Faculty of Science and Engineering

Åbo Akademi University, 2024

Pihl Joachim, 2024. *The dyke porphyries in Kiirunavaara – geology, geochemistry, and mineralogy.* Master's thesis in geology and mineralogy. Faculty of Science and Engineering, Åbo Akademi University. This thesis was carried out in collaboration with LKAB.

ABSTRACT

The Kiirunavaara iron oxide-apatite (IOA) ore deposit in the Norrbotten county of northern Sweden is well-known worldwide as it has been studied extensively throughout decades and is the largest IOA deposits known to this day. The subject of this thesis is a group of porphyry dykes (DPs) that irregularly intrude the Kiirunavaara footwall rocks and ore body to then disappear into the hanging wall rocks. The up to >10m wide dykes varies from red, green to dark colours and comprise pale glomerocrysts of feldspar often together with clinopyroxene, amphibole, and titanite, in an aphanitic groundmass. Variation in groundmass colours represent ratios of green silicates clinopyroxene and amphibole to iron oxide staining of the fine-grained feldspar matrix, resulting in sample groundmasses to be either green or red, respectively. Replacement of green silicates by biotite represent dark coloured samples.

The volcanic silicate host rocks to the Kiirunavaara iron ore are extensively Na-metasomatically altered, including the DPs. Geochemical major element classifications plots show that the DPs in a range from intermediate trachyandesite to a felsic rhyolitic composition, largely overlapping both hanging wall and footwall rocks. However, in immobile trace element diagrams they plot essentially in the rhyolitic/dacite fields, again overlapping completely with the hanging wall rocks, while foot wall rocks are separated into the andesite fields. The DPs, together with the volcanic porphyries, plot as metaluminous indicating metaigneous sources, and geotectonic discrimination diagram using Ta/Yb v. Th/Yb show a dominantly active continental margin environment for the DPs. A LA-ICP-MS U-Pb zircon age determination of one sample yielded a concordia age of 1880±4 Ma (MSWD=0.79; n=26), which represent the DPs crystallization age.

Results from this thesis concludes the fact that the dyke porphyries of Kiirunavaara share inseparable textural characteristics with the hanging wall rocks as well as completely overlapping each other geochemically and fall within the same age range. Therefore, the DPs are closely associated to the volcanic evolution of Kiirunavaara, representing magmas of identical composition to the hanging wall volcanics and interpreted as feeder channels to that volcanism. Intrusions of DPs occurred in an active continental margin environment and crosscutting relations to the ore body indicate pulses of DP-magma to occur at the waning stages of footwall and ore magmatism. Geochemical differences in green and red DPs suggest they originate from separate magma pulses.

TABLE OF CONTENTS

Appendices

1 INTRODUCTION

Kiirunavaara and its associated well-known Paleoproterozoic apatite iron ore body and host rocks are located in northern Sweden, as a part of the Fennoscandian Shield (e.g., Martinsson et al. 2016). The dyke porphyries (DPs) in Kiirunavaara are fine-grained porphyritic rocks forming complex intrusive patterns within the footwall and through the ore body but disappearing into the hanging wall volcanic porphyries (Geijer 1910a; 1960; Andersson 2013).

Geijer (1910a) first described the dyke porphyries at the time as syenite porphyry dikes and their geological position in Kiirunavaara. Later, the dyke porphyries and their geological position have been discussed, but no studies focused on the dyke porphyries describing them in detail have been conducted. Thus, this thesis aims to describe the dyke porphyries in some detail, characterizing their occurrence, age, mineralogy, geochemistry, and to compare them with relevant surrounding rock types for inferences on their position and origin to be made. Zircon geochronology of one sample is included. This task is important as it could improve the understanding of the geological evolution of the rock types closely associated with the ore and, thus, the setting in which the Kiruna-type ores have formed.

The dyke porphyries share many textural similarities with the hanging wall porphyries but are distinct from the footwall porphyries which they invariably crosscut. Based on these characteristics, it has been implied that the DPs may represent feeder dykes to (at least parts of) the hanging wall volcanism (Geijer 1919; Andersson 2013). This thesis will add some data to further test this possibility.

One conspicuous feature of the dyke porphyries is that they display different varieties in the colour of the groundmass, where the most common appear to be red and green but grey/dark varieties also occur. The origin of this will also be addressed.

In this study, a set of samples of dyke porphyry and a few samples of hanging wall porphyry will be described petrographically, using microscopy with transmitted and reflective light. Geochemical analysis of major and trace elements will be performed on the samples and compared with data from the LKAB geochemical data base, to unravel chemical characteristics. In addition, zircon U-Pb geochronology of one dyke porphyry sample will be performed. A synthesis discussion on the position and origin of these dykes will be presented.

2 GEOLOGICAL BACKGROUND

2.1 Regional geology

The Kiirunavaara ore body is located in the Norrbotten county of northern Sweden as a part of the Fennoscandian Shield (Fig. 1). Norrbotten county is one of Europe's most important mining areas, being intensely mineralized especially in its northern parts (e.g., Martinsson et al. 2016). The Norrbotten regional geology consists of an Archean (2.8 – 2.6 Ga) basement which is exposed in the northern and southernmost parts of the area. Overlying the Archean basement is early Paleoproterozoic (2.5 – 2.0 Ga) supracrustal rocks lithostratigraphically referred to as Karelian, and Paleoproterozoic (2.0 – 1.8 Ga) supracrustal rocks lithostratigraphically referred to as Svecofennian. Major magmatic suites have intruded the area at about the same time as the 2.0 – 1.8 Ga Svecokarelian orogeny, which have affected all Precambrian rocks in the area to some extent (see Bergman & Weihed 2020 for overview).

Archean rocks are mostly exposed in the northernmost part of Norrbotten, northwards from Kiruna, where they form the Råstojaure complex of mainly tonalitic to granodioritic orthogneisses with a formation age of 2.8 – 2.7 Ga (Martinsson et al. 1999), but also metagranites crystallized at 2.7 are common in the eastern parts. In the southern part of Norrbotten smaller areas of exposed Archean rocks are found, mainly 2.6 Ga banded gneisses ranging from granitic to quartz monzonitic in composition, and 2.7 – 2.6 Ga metamorphosed monzodiorite to granodiorite (Mellqvist et al. 1999, as cited in Bergman & Weihed 2020). Within the Råstojaure complex, some early Paleoproterozoic 2.5 – 2.4 Ga ultramafic – mafic intrusive rocks are also found (Bergman & Weihed 2020, and references therein).

Unconformably overlying the Archean basement are the Paleoproterozoic Karelian (2.5 – 2.0 Ga) and Svecofennian (2.0 – 1.8 Ga) units. The Karelian unit consists of a stratigraphically lower subunit, the Kovo Group (2.5 – 2.3 Ga), of mostly basal siliciclastic metasediments and tholeiitic metabasalts, which is unconformably overlain by the Kiruna Greenstone Group (2.3 – 2.0 Ga) of mostly metamorphosed tholeiitic basalt, some komatiite, and metasediments (Fig. 2) with origins in an extensional tectonic setting (e.g. Martinsson 1997; 2004; Bergman & Weihed 2020).

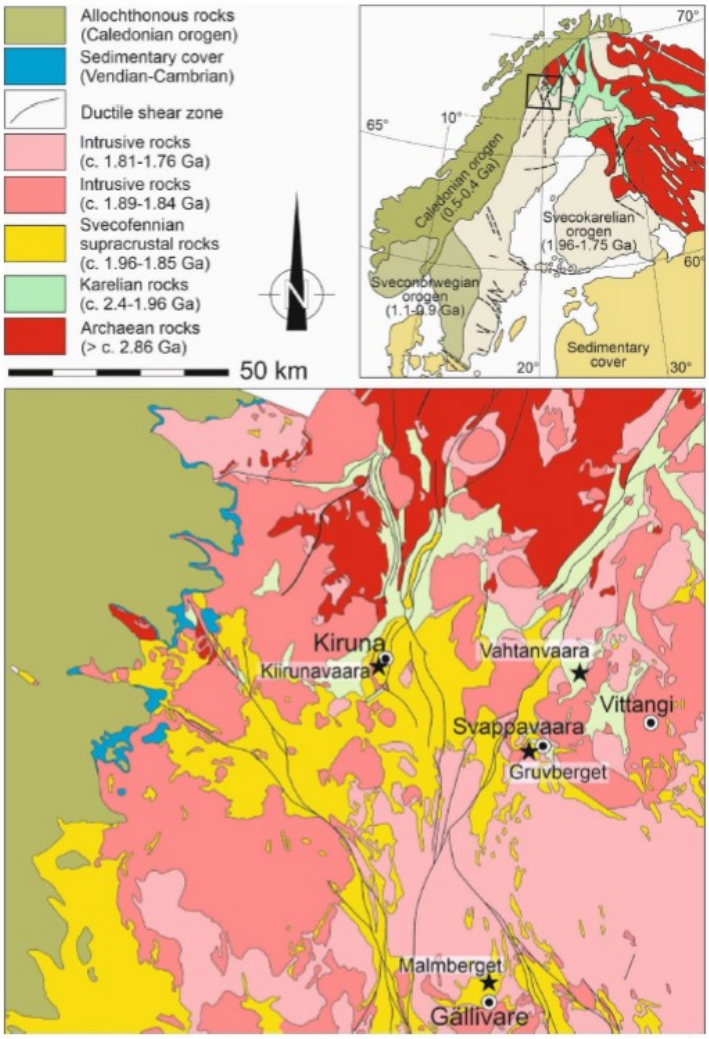

Fig.1. Geological map of northern Norrbotten (modified from Bergman et al. 2001 by Gilg & Andersson 2020).

The Karelian units are unconformably overlain by the Svecofennian units, which are composed of volcanic and sedimentary rocks of Svecofennian age (e.g., Martinsson 2004). The Kurravaara conglomerate represents a clastic basal sedimentary facies unit with minor intercalations of volcanic rocks, while the Porphyrite group is dominated by volcanic, mainly andesitic rocks. The Porphyrite group volcanic rocks have been considered to indicate a change to convergent tectonics (Martinsson et al. 2016), and Andersson et al. (2021) advocate an intracontinental back-arc environment at the time of emplacement of the volcanic rocks and the associated ores. Following upwards in the stratigraphy comes the Kiirunavaara Group, also referred to as the Porphyry group, mainly consisting of intermediate to felsic volcanic rocks. This unit is further divided into three formations called the Hopukka, Luossavaara, and Matojärvi formations (Martinsson 2004).

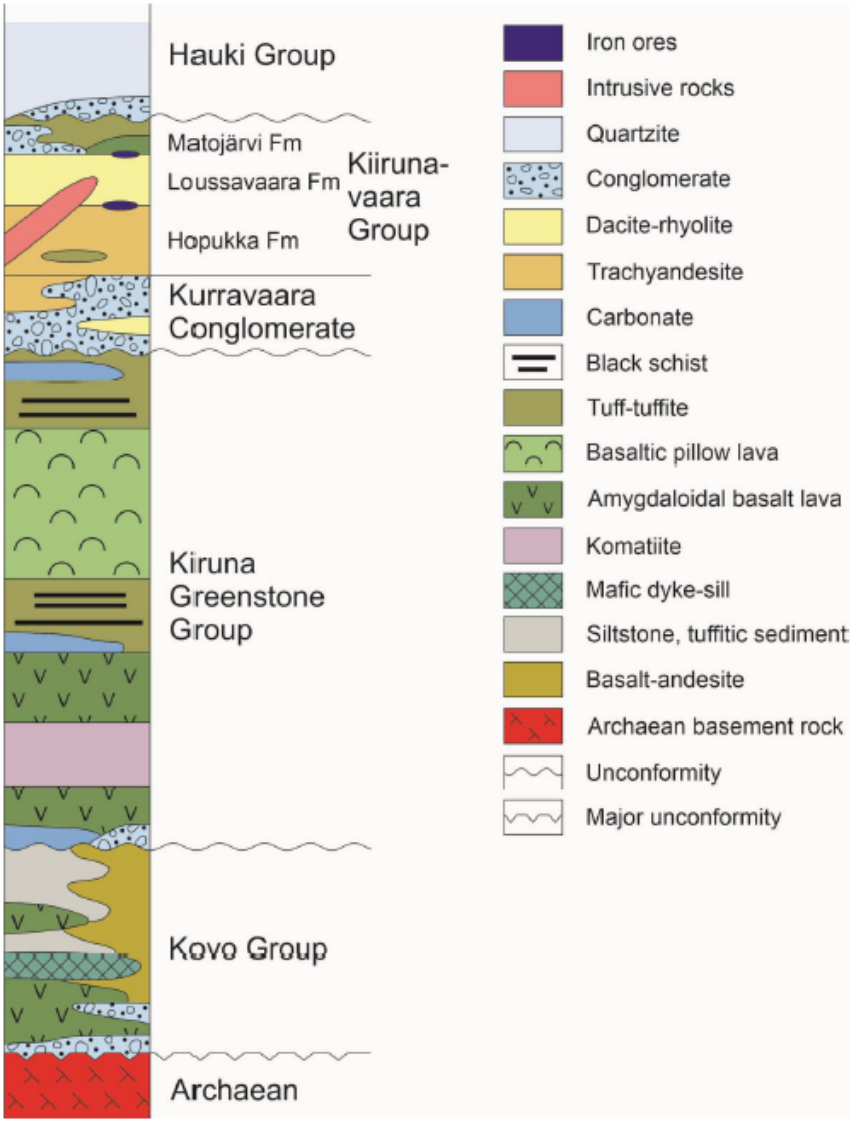

Fig. 2. Simplified lithostratigraphy of the Kiruna area (modified from Martinsson et al. 2016 by Gilg & Andersson 2020).

The Hopukka and Luossavaara formations consist of mildly metamorphosed trachyandesitic lava flows and porphyritic (pyroclastic) rhyodacite, respectively. They have traditionally been called syenite porphyry and quartz-bearing porphyry (e.g., Geijer 1910; 1960). The Matojärvi formation furthest up in the Kiirunavaara Group comprise a lower volcanic part called the "Rektor porphyry" (Geijer 1910a; 1950) of K feldspar-altered felsic tuff, overlain by basalts and a sedimentary sequence of conglomerate and pelitic rocks (Martinsson & Erlandsson 2009; Martinsson et al. 2016; Andersson et al. 2019). The Kiruna apatite-Fe oxide deposits are found within the Kiirunavaara Group (Martinsson et al. 2016, 2004; Bergman & Weihed 2020). The Hauki Quartzite constitutes the uppermost part of the Svecofennian units, being

deposited after 1.88 Ga (Bergman & Weihed 2020) and indicating a change from a volcanic environment to epiclastic sedimentation (Martinsson et al. 2016). It is mainly composed of quartzite/metaarkose and metaconglomerate and lies disconformably over the Luossavaara and Matojärvi Formations (Frietsch 1979; Martinsson et al. 2016; Bergman & Weihed 2020).

Intrusive rocks emplaced in the Norrbotten region at 1.89 – 1.86 Ga, syn-orogenic relative to the Svecokarelian orogeny, include the Haparanda suite and the Perthite monzonite suite (e.g., Witschard 1984). The gabbroic to granitic Haparanda suite is deformed, whereas the Perthite monzonite suite is mainly isotropic or less deformed, indicating a slightly younger age compared to the Haparanda suite (Bergman & Weihed 2020). The youngest major magmatism in the area is represented by the Lina suite which formed at c. 1.8 Ga (e.g., Sarlus et al. 2018; 2020). It is mainly composed of granite, associated with pegmatite, and also occurs as dykes in older rocks (Bergman & Weihed 2020).

2.2 Local geology of Kiirunavaara

In the northern part of Norrbotten county, there are about 40 known apatite iron ore deposits (Martinsson et al. 2016). The ores are hosted by the volcanic rocks of the Kiruna porphyries including the Kiirunavaara group and the Porphyrite group. In the central Kiruna area, several apatite iron ore deposits are situated. Kiirunavaara, mined by LKAB (Luossavaara – Kiirunavaara Aktiebolag), is the largest deposit with an estimated pre-mining total of >2 000 Mt of ore (e.g., Martinsson 2004). Some other deposits are the Luossavaara deposit and the "Per Geijer ores": including Rektorn, Haukivaara, Nukutus, and Henry deposits, which are presently not mined but under exploration (Bergman et al. 2001; Hilmo et al. 2022).

2.2.1 The apatite iron ores

The apatite iron ores show a range of varieties between and within the individual deposits. Iron contents are on average between 30 and 70% and the phosphorous contents between 0.05 and 5% (Niiranen 2006; Bergman et al. 2001). Furthermore, the iron ores differ regarding host rock lithologies, associated minor components and alterations. Two different types of deposits can be distinguished, breccia iron ores and stratiform – stratabound iron ores (Martinsson et al. 2016).

The breccia type iron ores occur in the lower parts of the Porphyry group or in the Porphyrite group mainly within intermediate to mafic volcanites. Characteristic for this type of ore is low iron and phosphorus contents and magnetite being the main iron oxide. Still apatite is one of

the most common gangue minerals (Lundberg & Smellie 1979) and other consistently present minerals are amphibole and mainly titanite, chalcopyrite, and pyrite as accessory minerals. The Mertainen deposit belongs to this type (Lundberg & Smellie 1979). Albite and scapolite host rock alterations are reported to be most common for this type deposits (Bergman et al. 2001).

The stratiform – stratabound iron ores occur in the upper parts of the Porphyry group. These ores characteristically have higher contents of phosphorus, and hematite as the major iron oxide, with varying amounts of magnetite (e.g., Parák 1975; Andersson et al. 2019). Major gangue minerals are apatite, quartz, mica, and carbonate, and contrary to the breccia type ores amphibole is absent. Common alterations of the host rock are carbonate, biotite, tourmaline, and sericite. The Per Geijer ores are a part of this group (Parák 1975; Bergman et al. 2001).

Kiirunavaara hosts one of the largest apatite iron ores in the world, with a length of 4 – 5 km and widths up to 200 m, extending to depths of at least 2 000 m (e.g., Andersson & Rutanen 2016). The Kiirunavaara ore shares features with both iron ore types and magnetite is the major iron oxide. The partly tabular but irregularly shaped ore body has stratabound characteristics, but breccias occur along contacts with the wall rocks (Martinsson & Hansson 2004; Bergman et al. 2001). The ore contacts with the trachyandesitic footwall and the rhyodacitic hanging wall are in places sharp, but dykes and inclusions of ore in the country rocks are common (Geijer 1968; Andersson 2013; Andersson & Rutanen 2016). Alterations along the ore - wall rock contacts are in places extensive. Albitization is common in the footwall together with magnetite, actinolite and titanite (Geijer 1910a). Actinolite frequently occurs in the footwall and hanging wall contacts as an alteration mineral and biotite – chlorite alterations occur in certain parts of the hanging wall (Bergman et al. 2001). Strong albitization in the host rock closest to the ore contact has been observed, as well as Ca-Fe alterations, and cut by actinolite, as veins and disseminations (Paolillo & Giapis 2021; Lupoli et al. 2022). Biotite – magnetite -, epidote, and anhydrite veins are also common in the most proximal parts of to the ore contact and can be observed to cut the actinolite – albite alterations. Furthermore, large zones of clay alteration occur especially in the southern part of the Kiirunavaara deposit (Berglund & Andersson 2013). These clay-altered areas occupy both ore and its host rocks causing problematic conditions for mining as the rock mechanical properties are affected (Björnell et al. 2015). The clay mineral montmorillonite constitutes the most part of the clay alteration zones, as well as occasional illite-smectite (Gilg & Andersson 2020).

In mining at Kiirunavaara, the iron ores are distinguished into five types based on the phosphorus and iron contents (Niiranen 2006). The phosphorus-low B ore with less than 0.05% P is further subdivided into an iron-rich B1 and an iron-poor B2 classification. The

latter is typically enriched in various silicates, including actinolite, phlogopite, chlorite and talc (Nordstrand & Andersson 2013; Aupers 2014). The phosphorus-rich D ore with more than 0.1% P is subdivided into D1, D3, and D5 according to increasing P content (Niiranen 2006). U-Pb zircon geochronology of the Kiirunavaara ore has yielded a concordia age of 1874 ± 7 Ma (Westhues et al. 2016).

Since the late 19th century (e.g., Löfstrand 1891; Geijer 1910b), the origin of the apatite iron ores of Lapland has been debated with several genetic models and is yet to be fully understood and agreed upon (cf. e.g., Parák 1975a; Frietsch 1984; Nyström 1985; Hitzman et al. 1992; Smith et al. 2009; Andersson 2013; Troll et al. 2019). Geijer (1910a) proposed a magmatic origin describing ore emplacement from differentiated iron oxide magmas. Later a sedimentary volcanic-exhalative model was proposed by Parák (1975b). Ore formation from hydrothermal fluids provided by adjacent intrusions (Westhues et al. 2016; 2017) is advocated by some, while others maintain a magmatic/magmatic-hydrothermal origin (Nyström et al. 2008; Troll et al. 2019), possibly involving assimilation of evaporites (Peters et al. 2022).

2.2.2 Footwall rocks

The (sub)volcanic footwall rocks of the magnetite ore form part of the Hopukka formation in the lower Porphyry group (Martinsson 2004). The c. 700 m succession constitutes several trachyandesitic lava flows as well as some intrusive bodies (Geijer 1960, Bergman et al. 2001; Westhues et al. 2016). The traditional terminology for the trachyandesite footwall (Bergman et al. 2001), described by Geijer (1910a) as syenite porphyries, is used in the mine. Geijer (1910a) described compositional and textural varieties from a medium-grained syenite transitioning upwards through fine-grained varieties into the syenite porphyries, as well as a nodular syenite porphyry variety. The footwall rocks vary from a greenish grey to reddish colour, with an aphanitic groundmass dominated by feldspars (albite, K-feldspar) along with amphiboles, magnetite and titanite (Geijer 1910a; Sandberg 2018). Phenocrysts of feldspar in the syenite porphyry are commonly pale grey greenish, with a size of about 1-3 mm. Amphibole phenocrysts also occur to a lesser extent (Geijer 1910a). The nodular syenite porphyry is particularly common near the ore (e.g., Andersson 2013) and consists of prominent rounded nodules of amphibole, titanite, magnetite, apatite, and mica, etc., often with dimensions of a few mm, occasionally up to 1 dm, but typically <1 cm (Palm 2015; Gray 2016). Small veins of the nodule-forming minerals are common (Geijer 1910). Alteration minerals of the footwall are, according to Geijer (1910a), amphibole, titanite, epidote, and chlorite. The amphibole through uralitization from augite, with primary hornblende/actinolite - tremolite being present in the nodules and fissures (Palm 2015). Zircon grains are limited in

the footwall rocks but have been U-Pb dated to a $^{207}Pb/^{206}Pb$ weighted mean age of 1884 ± 4 Ma and a concordia age of 1877 ± 12 Ma (Westhues et al. 2016).

2.2.3 Hanging wall rocks

Further up in the Porphyry group overlying the Hopukka formation comes the Luossavaara formation, where the c. 800 m thick succession of volcanic porphyritic hanging wall rocks is located (Martinsson et al. 2016). This unit is considered to consist of different eruptive beds and contain enclaves of rocks lower in the stratigraphy (Geijer 1968). These felsic porphyries, interpreted mainly as pyroclastic flows in origin, are rhyodacitic in composition and comprise abundant 2-5 mm feldspar phenocrysts/glomerocrysts (e.g., Ekström & Ekström 1997; Martinsson et al. 2016; Sandberg 2018). Some phenocrysts of augite occur, and inclusions of magnetite and amphibole can be observed in phenocrysts. Geijer (1910a) originally termed the rocks "quartz porphyries" due to the aphanitic groundmass of mainly feldspar and quartz, even though quartz phenocrysts are lacking, but later changed the term to "quartz-bearing porphyry" (e.g., Geijer 1931). Other than about similar quantities of feldspar and quartz, some magnetite, amphibole, biotite, titanite and apatite occur in the often red to grey groundmass (Geijer 1910a; Berglund et al. 2010; Sandberg 2018). Alterations of the hanging wall rocks show a transitional evolution from a Na-alteration (albite) closest to the ore body followed by a Na-Ca (albite, actinolite, titanite, epidote) continuing to a Na-Ca-Fe (albite, actinolite, magnetite) and finally to a distal K-Fe (biotite, magnetite) alteration (Paolillo & Giapis 2021; Lupoli et al. 2022). Contrary to the trachyandesitic footwall rocks, the felsic hanging wall rocks are abundant in zircons. Two samples with numerous zircon grains have been dated by U-Pb concordia ages at 1879.5 ± 7.1 Ma and 1880.5 ± 4.5 Ma, and a more altered sample with fewer grains yielded a $^{207}Pb/^{206}Pb$ weighted mean age of 1880.1 ± 2.7 Ma (Westhues et al. 2016). The hanging wall rocks share textural properties (Sandberg 2018) with the by Geijer (1910a) described syenitic dyke porphyries (although his analyses do not show syenitic compositions) that are passing through the footwall and ore body.

2.2.4 The dyke porphyries

The dyke porphyries, which are the subject of this thesis and described in more detail below, were first described by Geijer (1910a) as syenite porphyry dikes within the footwall unit and later as dyke porphyries (Geijer 1960). These dyke porphyries occur in Kiirunavaara running in general east – west, but also along the stratigraphic layering (near-north-south; see below) and have been observed to cut the footwall rocks and the ore body in many locations, as well

as being ‘broken up’ by the ore (Fig. 3; see also Aspvik 2000). The cutting relations indicate intrusions of dyke porphyries both before and after ore placement, according to Geijer (1910, 1919, 1960), as well as contemporaneous, resulting in magma mingling structures with ore, according to Andersson (2013). The dyke porphyries consist of rounded, pale feldspar phenocrysts in an aphanitic groundmass. Phenocrysts composed of several crystals, so called glomerocrysts, generally occur (Geijer 1910a, Sandberg 2018). Phenocrysts of hornblende and augite are also present (cf. Lindgren 2013). The groundmass is dominated by feldspar, but with hornblende and augite in some cases making up more than one third of the mass. Small grains of quartz and apatite occur sparingly and magnetite as well as titanite are less common than in the older porphyries, according to Geijer (1910a). The dyke porphyries show similar textural properties as the hanging wall quartz-bearing porphyries and have not been observed to crosscut the latter but seem to disappear into these without separable contacts. Unlike the syenite porphyries of the footwall, which they penetrate, the dyke porphyries seldom display individual rectangular feldspar phenocrysts and lack the common type of nodules observed in the syenite porphyries (Geijer 1910a).

Fig. 3. Dyke porphyry as rounded enclaves in ore on top of northern Kiirunavaara (Photo Ulf B Andersson).

3 MATERIAL

3.1 Samples and reference material

Samples for this study were collected from 18 different localities in the Kiirunavaara mine, 14 of which were collected from dyke porphyries and four from the hanging wall quartz-bearing porphyries. For the study to be as diverse as possible the samples were collected from different levels and blocks of the mine (Maps of collected sample locations in the Appendix). Samples of dyke porphyries were collected for the purpose of geochemical analyses and thin sections for petrography/mineralogy. One sample of dyke porphyry was collected specifically for geochronology, in addition to geochemical analysis and optical microscopy. The quartz-bearing porphyry samples were collected for comparisons to be made with the dyke porphyries. Two quartz-bearing porphyry samples were collected for geochemistry and thin sections, and two samples of contact relations of the quartz-bearing porphyry and the ore were collected for thin sections. Most of the sampling was done in January 2022 together with Ulf B Andersson and Etienne Lindborg Bordenave at LKAB.

From LKAB´s database geochemical data of relevant local lithologies, a total of 21 838 analyses, for comparisons to be made against results from this study have been available. Other material available for this study are thin sections from Lindgren (2013) and Sandberg (2018).

3.2 Sample preparations

From the 18 sample localities, a total of 22 thin sections were prepared by sawing them to correct sizes to then be polished and made into thin sections by laboratory technician Arto Peltola, Turku.

Samples for geochemical analysis were crushed and milled to then be sent to ALS laboratories for major- and trace element analysis.

For age determination one sample of dyke porphyry was collected from a larger dyke in the footwall at level 1223, with the coordinates X6400 Y2120 Z1223, using the local coordinate system of LKAB. The sample was collected by Ulf B Andersson in November 2021.

About 2 Kg of the collected sample was used in the mineral separation process. Zircons were extracted from the sample using standard mineral separation methods: crushing, milling, sieving, panning, hand magnet and heavy liquid. About 150 zircons and some unknown heavy minerals were handpicked under a microscope and mounted on double-sided tape to be made into a polished resin puck exposing a crosscut of the mineral grains.

4 METHODS

For petrographic descriptions of the samples, the polished thin sections were observed with transmitted and reflective light microscopy. Reflective light microscopy was used for the identification of opaque minerals. Sample pulps were sent to ALS Scandinavia AB preparation laboratory, and geochemical analysis to determine elemental composition performed with ICP-AES for major elements and ICP-MS for trace elements were conducted by ALS Geochemistry in Loughrea, Ireland. Plotting of geochemical data was done in the free program geochemical data toolkit (GCDkit) and in the data analysis software ioGAS by Imdex. To find out the age of the dyke porphyries and thus their position in the evolution of Kiirunavaara geology, U-Pb age determination using LA-ICP-MS was conducted on the zircon mount at the Geological Survey of Finland in Espoo. Backscattered Electron images and Cathodoluminescence images were pre-prepared and used to navigate the resin puck and choose appropriate locations for analysis on the zircons.

4.1 U-Pb geochronology

The principles of U-Pb geochronology are based upon the decay of the radioactive isotopes of uranium and their stable daughter isotopes of lead. The two radioactive uranium isotopes ^{238}U and ^{235}U decay to the lead isotopes ^{206}Pb and ^{207}Pb, respectively. The non- radiogenic common ^{204}Pb isotope is used to monitor the non-radiogenic lead in the sample. Zircon is the most frequently used U- and Th-bearing accessory mineral used in this method, due to its common occurrence in the earth´s continental crust. Zircon crystallizes under a variety of geological conditions, mostly at high temperature, and has physical and chemical properties to survive at low-temperature detrital conditions, as well as up to high temperature metamorphic and melting events (e.g., Hanchar, 2003; Harley & Kelly 2007). It often shows a complex pattern of zonation which may enable to record the mineral grain's geological evolution through time (e.g., Scherer et al. 2007). Cathodoluminescence (CL) and Backscattered Electron (BSE) imaging is most suitable to reveal these growth records. Upon crystallization, the crystal lattice of zircon readily incorporates U and Th, while it excludes Pb, making its ratio of U/Pb high and, thus, suitable for geochronology (Parrish and Noble, 2003 & Ireland and Williams, 2003).

4.2 LA-ICP-MS (Laser Ablation Inductively Coupled Plasma Mass Spectrometry)

U-Pb dating was performed with the analytical method LA-ICP-MS, using a Nu Plasma AttoM single collector ICPMS linked to a Photon Machine laser ablation system. Inside a HelEx ablation cell, the samples were ablated with He gas (Müller et al., 2009) and mixed with Ar gas before continuing into the plasma. Conditions for plasma ablation were set to a 20 μm beam diameter, 5 Hz pulse frequency, and a beam energy density of 2.17 J/cm^2. Every measurement was initiated with a short pre-ablation flushing of the ablation cell and an on-mass background measurement before the final ablation with a stationary beam. Prior to and at the end of the analytical session, calibration standards and in-house control samples were run, as well as within regular intervals during the session. Calibration standard used for the session was GJ-1 (609 ± 1 Ma; Belousova et al. 2006) and control samples A382 (1877±2 Ma, Patchett & Kouvo, 1986; Huhma et al., 2012) and A1772 (2712 ±2 Ma, Huhma et al., 2012). The program Glitter (Van Achterbergh et al., 2001) was then used to correct the raw data for background radiation, laser induced elemental fractionation, and mass discrimination. The data was calibrated to U-Pb isotope ratios using concordant references. An Excel spreadsheet, written by Y. Lahaye and H. O'Brien, was used to correct the data for common lead.

4.3 Geochemistry

Whole rock geochemical analysis and trace element analysis of the sample pulps were conducted by ALS laboratories. ALS offer their methods ME-ICP06 for major element analysis and ME-MS81 for trace element analysis. Prior to the whole rock methods, the minerals in the samples are broken down by a lithium borate fusion and acid dissolution, liberating all elements. The major rock-forming elements are then determined with an ICP-AES instrument. Trace elements are analyzed with ICP-MS (ALS, 2023).

For this study, a total of 18 samples were analyzed of which 16 were dyke porphyries (DP) and two hanging wall quartz-bearing porphyries (QP). These analyses were then compared to 455 DP, 11 313 QP and 10 070 syenite porphyry (SP) analysis from LKAB´s data base, analyzed with the same method and analytical procedure.

4.3.1 ME-ICP06 Whole rock ICP-AES

Inductively coupled plasma atomic emission spectroscopy (ICP-AES), or optic emission spectroscopy with inductively coupled plasma, is an analytical technique for detecting chemical elements at their different characteristic wavelengths. The plasma is created by using

argon gas in a partly ionised state, meaning it contains electrically charged particles which are achieved by letting the argon gas flow through a radio frequency field. This enables the plasma to reach extremely high temperatures of almost 10 000 °C. At these temperatures, elements will emit wavelengths of light characteristic for a particular element which are measured and analyzed for detection of element concentrations (ALS, 2023).

The sample enters the plasma as an aerosol of fine liquid droplets after which the different light wavelengths of the elements are separated using a lattice and picked up by detectors. This is a multi-element technique, which means that it can determine up to 40 elements at once. Detections limits in aqueous solutions for ICP-AES are typically at µg/l level (ALS, 2023).

4.3.2 ME-MS81 Lithium Borate Fusion ICP-MS

Inductively coupled plasma mass spectrometry (ICP-MS) is a highly sensitive technique for detecting elements and their different isotopes. This method uses the same kind of plasma as the ICP-AES described above. Elements in the analyzed sample are transformed into ions by the plasma to then be separated with mass spectrometry according to their mass-to-charge ratio. This enables measurements of element concentrations and separation of natural isotopes of the different elements (ALS, 2023).

Like the ICP-AES, ICP-MS is a multi-element technique combining characteristics from both methods, simple and fast sample handling of the ICP combined with the high sensitivity and isotope measurements achieved with mass spectrometry. Detection limits in aqueous solutions for ICP-MS are for some elements as low as ng/l levels (ALS, 2023).

5 RESULTS

5.1 Field observations and description

The dyke porphyries, present in the footwall and ore body of Kiirunavaara, occur irregularly as dykes from decimetre scale up to more than 10 meters wide. However, models of the mine geology show the occurrence of dyke porphyries to be concentrated in the central parts of the mine (Fig. 4). Typical contacts of the dykes and footwall rocks are sharp but often irregular whereas the contact with ore can be “brecciated” or “mingled”. Dykes show different colour

varieties from dark greyish to red and green (Fig. 7). These colour varieties occur as separate dykes as well as together in single occurrences (Fig. 8).

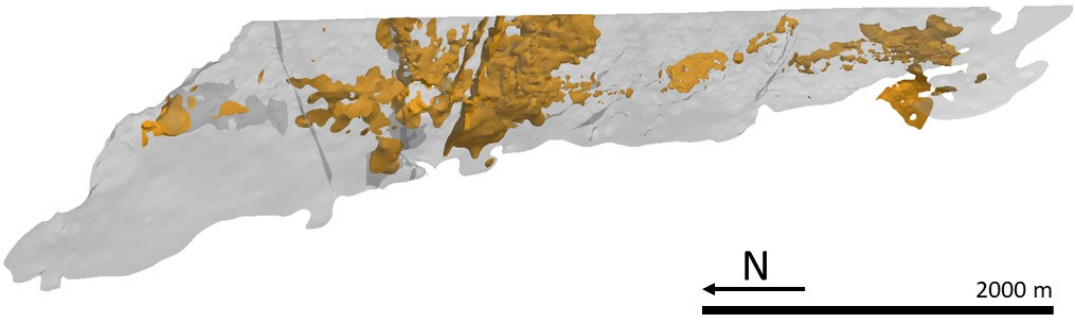

Fig. 4. Distribution of dyke porphyries (orange) in the ore body visualized looking from W to E. Model by Ann Bäckström

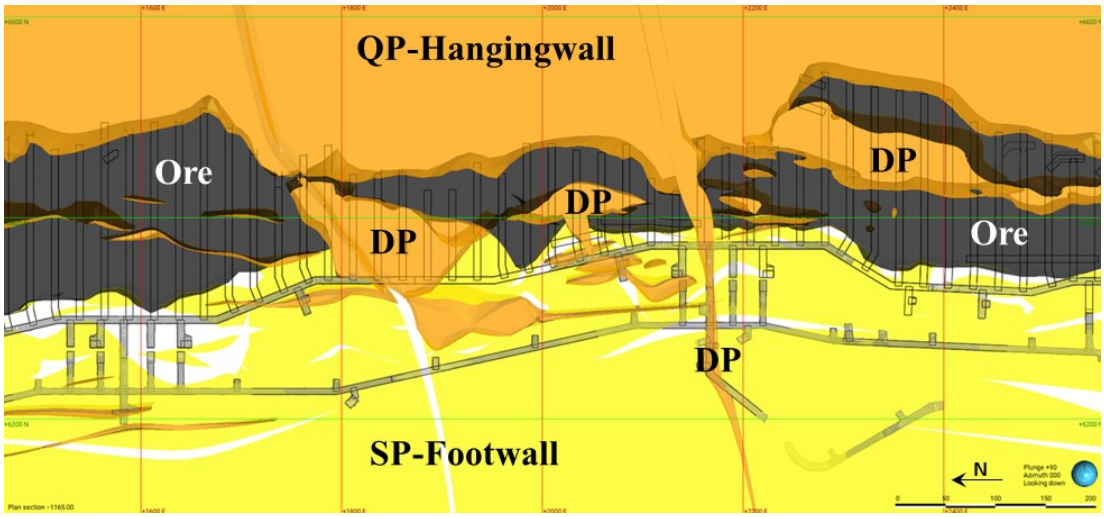

Fig. 5. Dyke porphyry distribution in the footwall and ore at level 1165 looking from above. Model by Ann Bäckström.

The dykes carry large 2-10 mm, pale coloured, phenocrysts of feldspars in an aphanitic groundmass varying in colour as described above. Dykes intrude the footwall rocks and ore body in an irregular way displaying sharp contacts (Fig. 6) but also mingling conditions especially with the ore (Figs. 3, 10, and 12). Although most of the tunnel walls were covered with shotcrete, spots where the dyke porphyries were exposed made sampling possible.

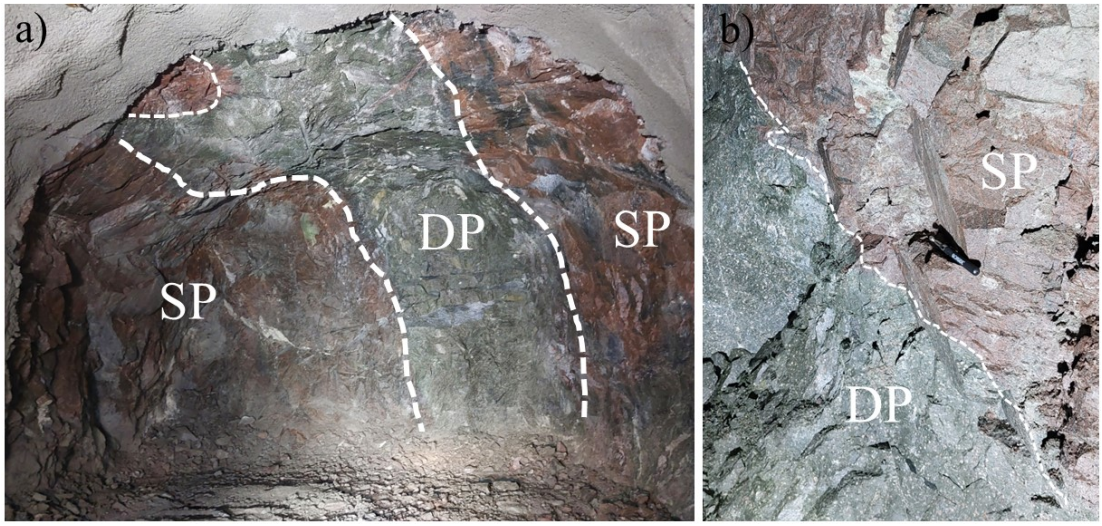

Fig. 6. (a) Typical dyke porphyry intrusive character in footwall, captured in block 41, level 1165, drift Ventort 33ST. (b) Sharp but irregular contact of DP in footwall porphyry in block 41, level 1165, drift Ventort 33SF.

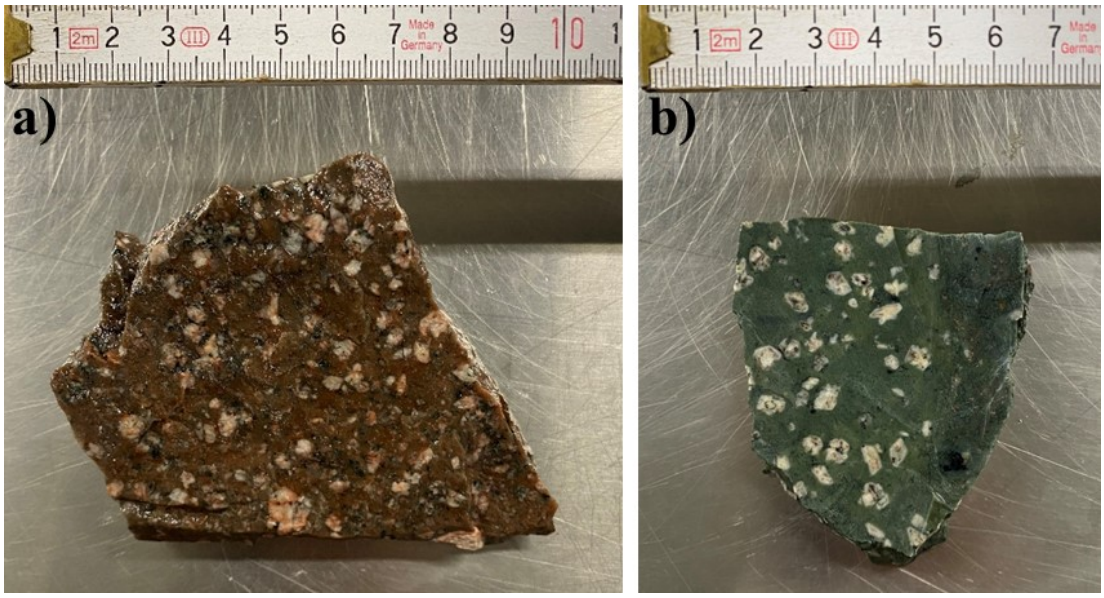

Fig. 7. Examples of dyke porphyry texture and colour variations, red (a) and green (b).

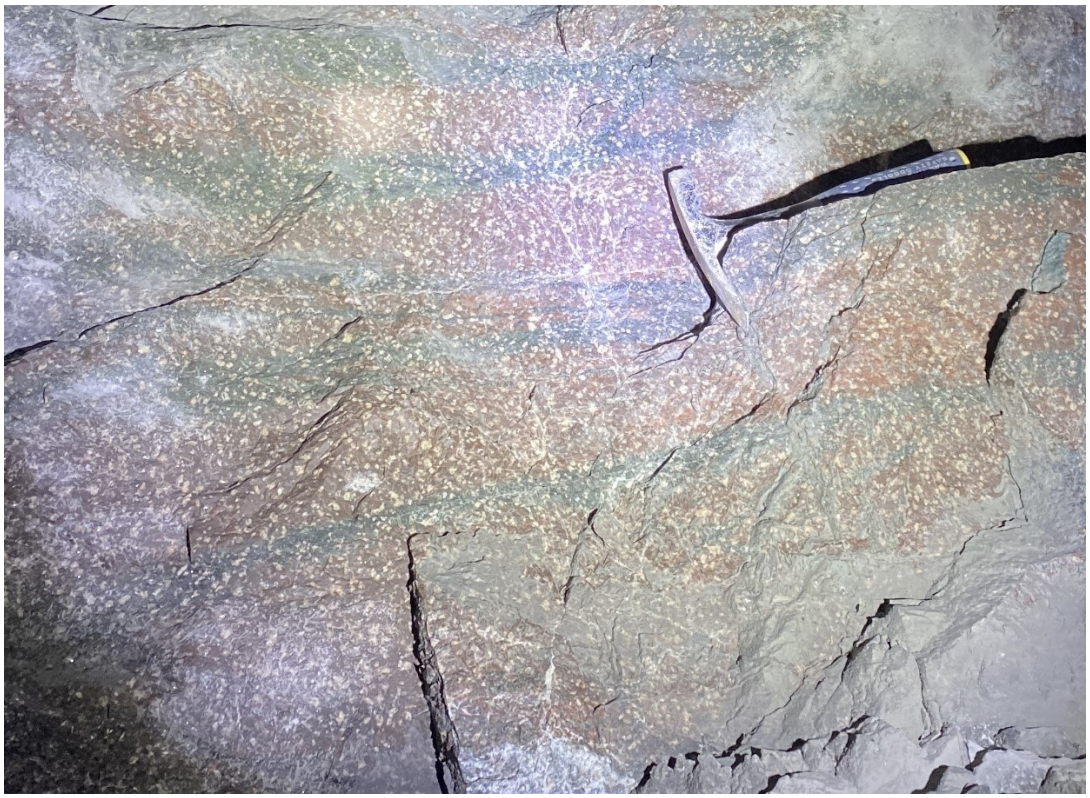

Fig. 8. Red and dark green colour variations in a single dyke (crosscut 139, level 1108).

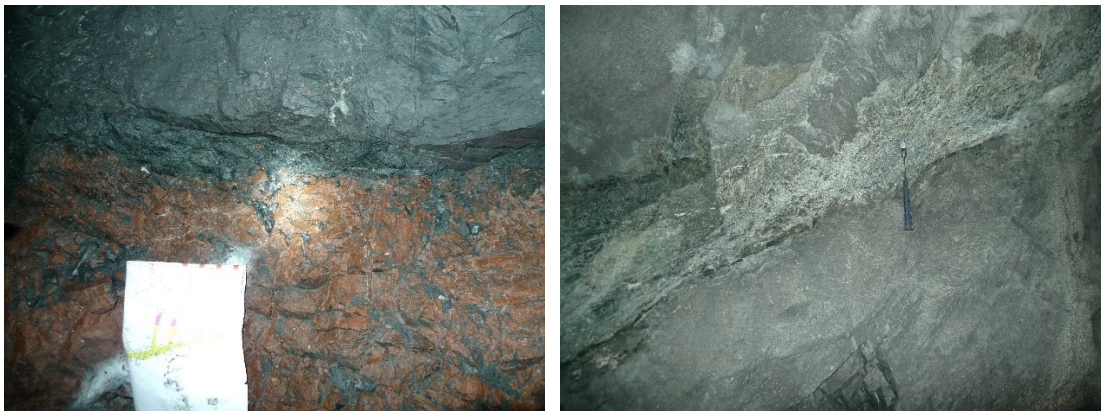

Fig. 9. A. Sharp contact between ore and QP (crosscut 316/level 1079). B. Clay-altered contact between ore and QP (crosscut 317/level 1051) (Photos: Ulf B. Andersson).

The hanging wall quartz-bearing porphyries show less variation than the footwall syenite porphyries. They are often red or dark in colour with pale phenocrysts, like the dyke porphyries. Ore-hanging wall contacts are often sharp, sometimes associated with alteration and shearing (Fig. 9). However, also 'brecciated' contacts occur where the ore has interacted with the quartz-bearing porphyry (Fig. 12) Nowhere have contacts between the dyke porphyries and the hanging wall porphyries been observed; thus, the dykes seem to merge into the hanging wall.

Fig. 10. (a) Hand sample of red quartz-bearing porphyry (from crosscut 335, level 1194). (b) Sample of red, altered quartz-bearing porphyry, showing interaction with ore, sampled at their contact (from crosscut 173, level 1165).

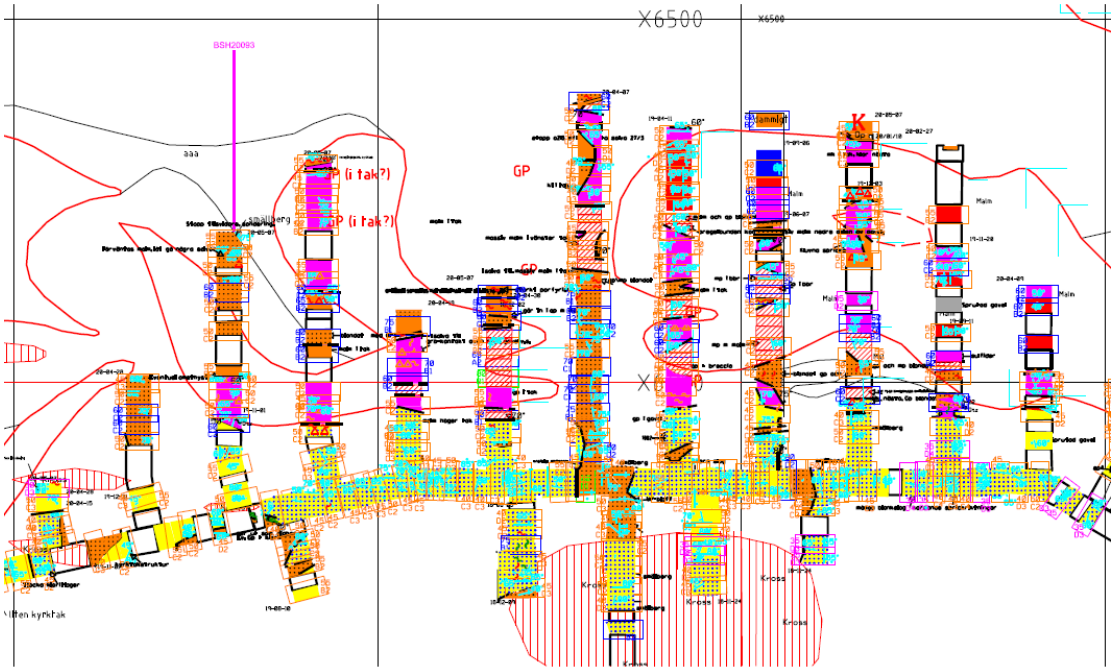

Fig. 11. Underground mapping from level 1165 block 22. Orange with black dots represent DP, irregularly transecting the footwall and ore.

Fig. 12. A. Example of interaction between DP and ore (crosscut 214/level 1137). B. Example of interaction at the contact between ore and QP (Crosscut 313/level 1137) (Photos: Ulf B Andersson)

5.2 Petrography

Dyke porphyries

The feldspar phenocrysts appear as pale, white to pinkish, few millimetres to even centimetre large euhedral to anhedral shapes and are commonly clustered together as glomerocrysts, together with other frequent minerals of the rock type such as clinopyroxene, amphibole and titanite (Fig. 13). The feldspars in the glomerocrysts show patchy and diffuse intergrowth of K-feldspar and plagioclase. Cross-hatched microcline and albite twinning is often seen intergrown in a perthitic or antiperthitic pattern (Fig. 14). Twinning is commonly absent. Feldspars are also the main constituents of the groundmass together with typically abundant quartz.

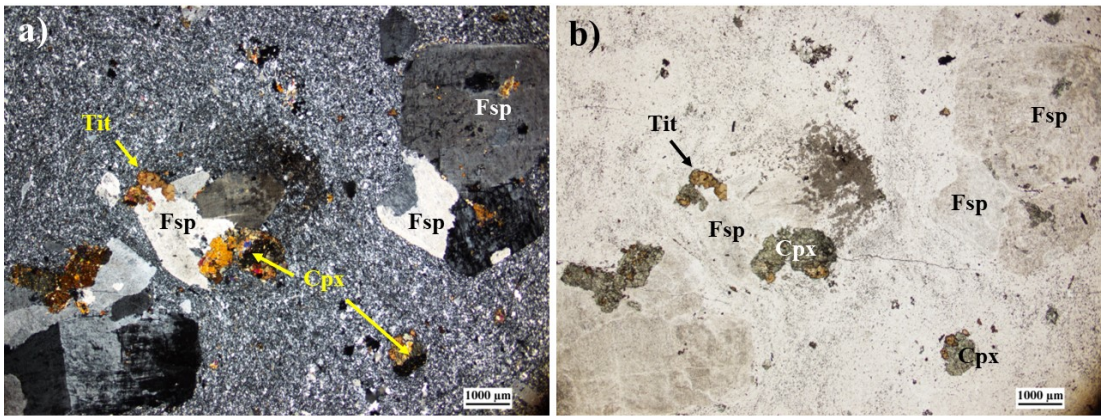

Fig. 13. Thin section of sample 217-1137 in cross polarized light (a) and plane polarized light (b). Glomerocrysts of feldspar, amphibole, and titanite in a fine-grained groundmass. Fsp = feldspar, Cpx = clinopyroxene, Tit = titanite.

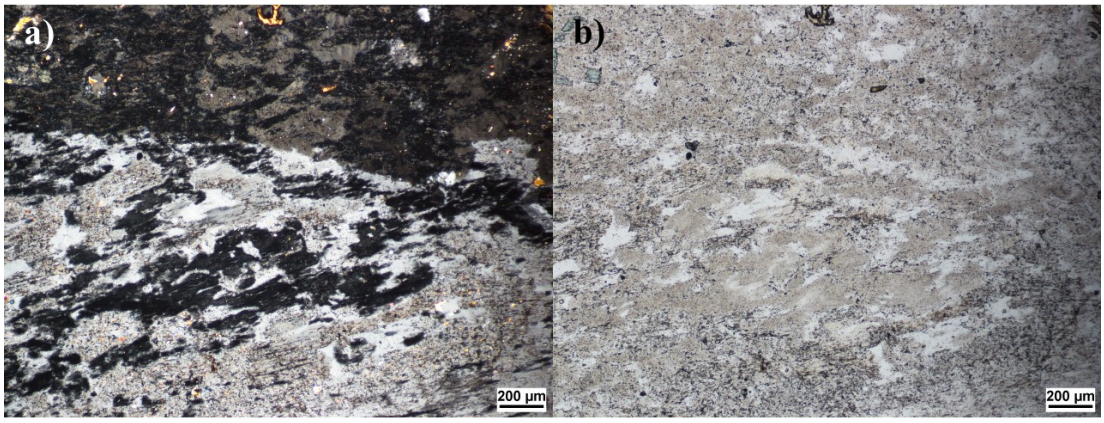

Fig. 14. Thin section of sample 139-1108a, showing typical textures in feldspars of the dyke porphyries. Photo zoomed in on a glomerocryst at boundary of two feldspar grains. Patchy intergrowth texture of K-feldspar and plagioclase in the bottom left. A) cross polarized light (xpl) and b) plane polarized light (ppl).

Other than feldspars the dyke porphyries are mainly composed of clinopyroxene and amphiboles both as phenocrysts, associated with the feldspar glomerocrysts and as main constituents of the groundmass (Figs. 15 and 18a). Clinopyroxene occur as brown anhedral blocky grains often partly altered into, or sometimes replaced by amphibole. The amphiboles appear as green irregular grains and as small needles in phenocrysts as well as in the groundmass. Titanite is present in all samples as rounded grains together with or as inclusions in the clinopyroxene, amphiboles, or in the groundmass.

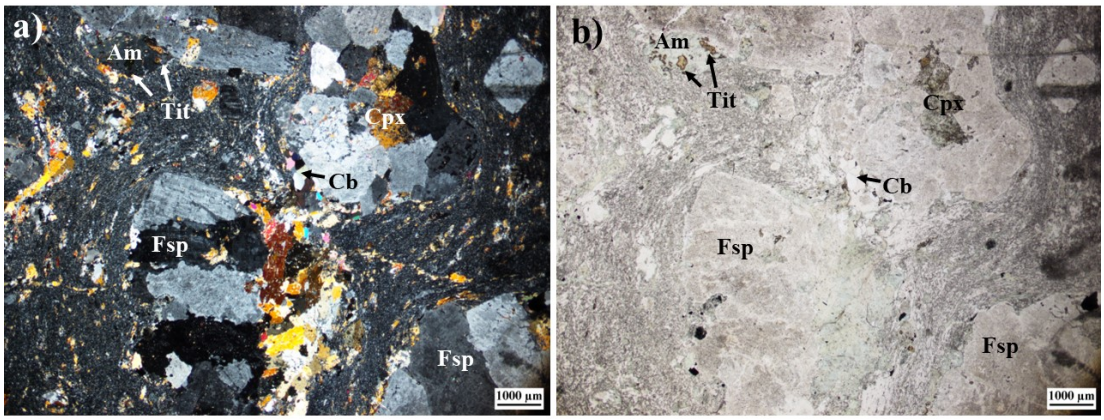

Fig. 15. Thin section of sample 139-1108c with glomerocrysts of feldspar, amphibole, titanite, clinopyroxene and carbonates in groundmass showing flow structures. Fsp = feldspar, Am = amphibole, Tit = titanite, Cpx = clinopyroxene, Cb = carbonate. A) in xpl and b) in ppl.

Quartz is present in the groundmass of all samples and sometimes occur as aggregates of larger grains in contact with phenocrysts (Fig. 16). Aggregates of carbonate, most likely calcite, occurs in most samples. Green biotite is sometimes present as slivers and at least one sample contain radioactive mineral inclusions in the biotite. Clinopyroxene and amphibole occur less or are absent in samples abundant in biotite. Anhydrite is present in most samples commonly in aggregates with carbonates. Other minerals that occur in smaller amounts are magnetite, pyrite, chlorite, apatite, and gypsum.

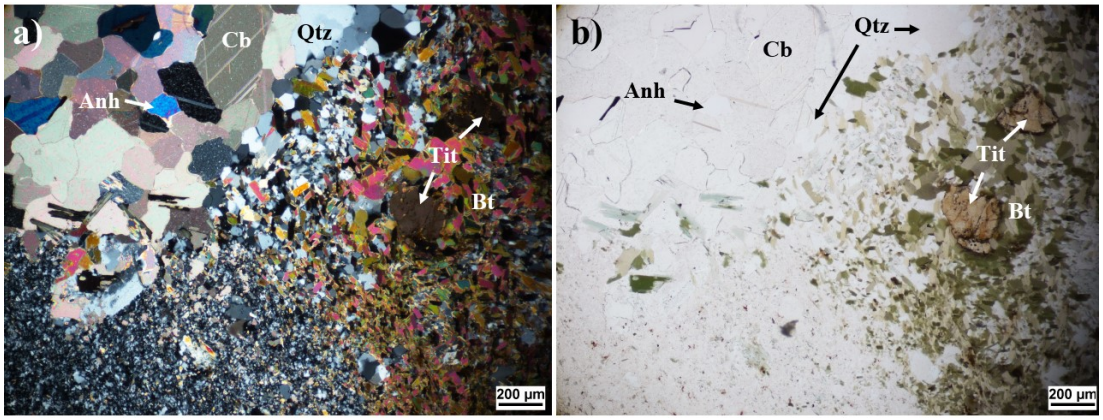

Fig. 16. Thin section of sample 137-1137 in both cross polarized light (a) and plane polarized light (b), with aggregates of carbonates, anhydrite, and quartz. Sample rich in green biotite. Titanite is also present. Cb = carbonates, Anh = anhydrite, Qtz = quartz, Bt = biotite, Tit = titanite.

The groundmass, mainly consisting of feldspar, clinopyroxene, amphibole, and quartz, show magmatic flow structures (Fig. 15, 17) in many of the samples. Some signs of possible pressure shadows indicating deformation are present in only a few samples. Variations in grainsize of the aphanitic groundmass can be observed. Samples with a green groundmass are dominated by the green silicates clinopyroxene and amphibole and typically show a less fine-grained groundmass than the red samples in which the groundmass contain less of the green silicates. Dark, almost black, areas of some samples seem to contain more biotite.

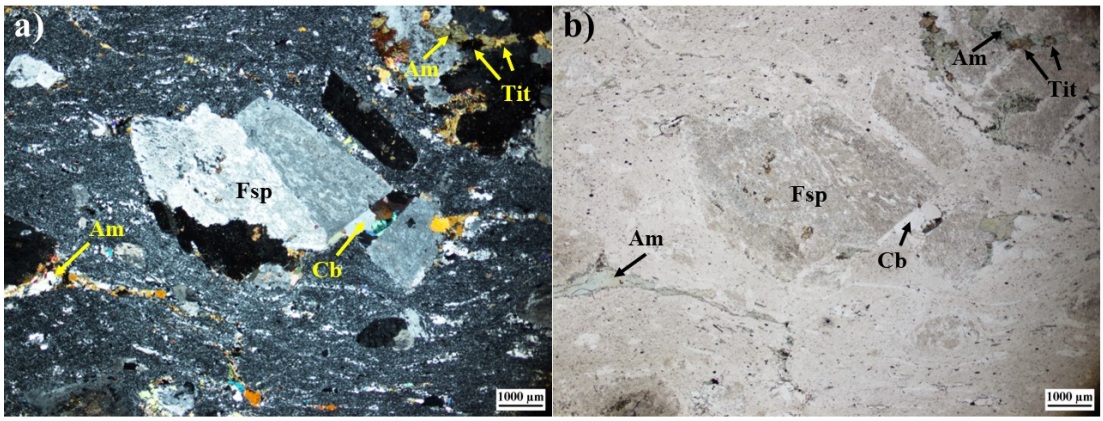

Fig. 17. Thin section of sample 139-1108a, showing magmatic flow structures in the groundmass around glomerocrysts of feldspar, amphibole, titanite, and carbonate. Possible pressure shadow in amphibole (bottom left). Cross polarized light (a) and plane polarized light (b). Fsp = feldspar, Am = amphibole, Tit = titanite, Cb = carbonate.

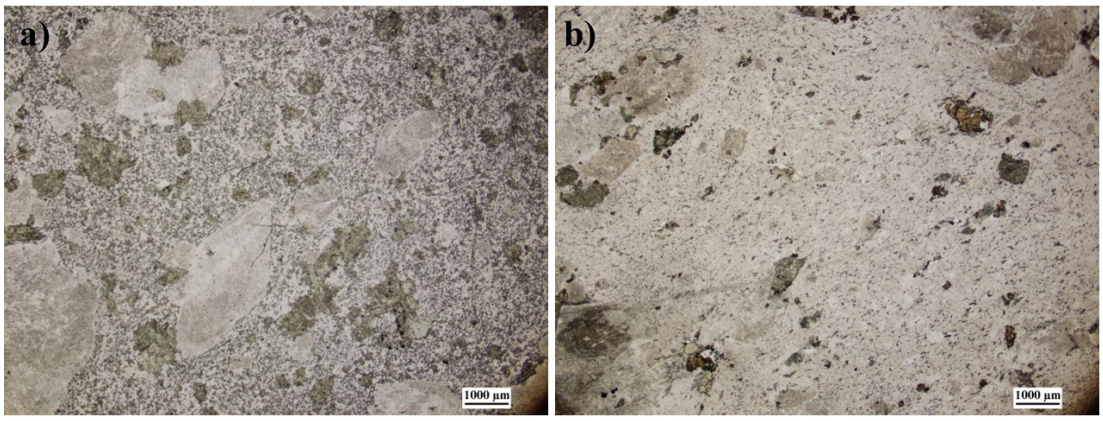

Fig. 18. Thin sections of samples 205-1108G (a) and 205-1108R (b) in plane polarized light. The green sample to the left shows a groundmass rich in green silicates clinopyroxene and amphibole, whereas the red sample to the right lack these in the groundmass and instead show reddish colour from iron oxide alteration of feldspars.

Quartz-bearing porphyries

The hanging wall quartz-bearing porphyry samples share almost inseparable textures and mineral composition with the dyke porphyries (Fig. 19, 20). They carry pale feldspar glomerocrysts in an aphanitic groundmass of feldspar, clinopyroxene, amphibole and quartz. Quartz seems to be somewhat more abundant in the groundmass of the quartz-bearing porphyries than in the dyke porphyries. Red is the most common colour of the groundmass, but dark grey varieties also occur. Like in the dyke porphyries, titanite, biotite, calcite, anhydrite, and magnetite also occur. Clear flow structures can be observed and the two samples from the contact between ore and hanging wall show complex contact relations.

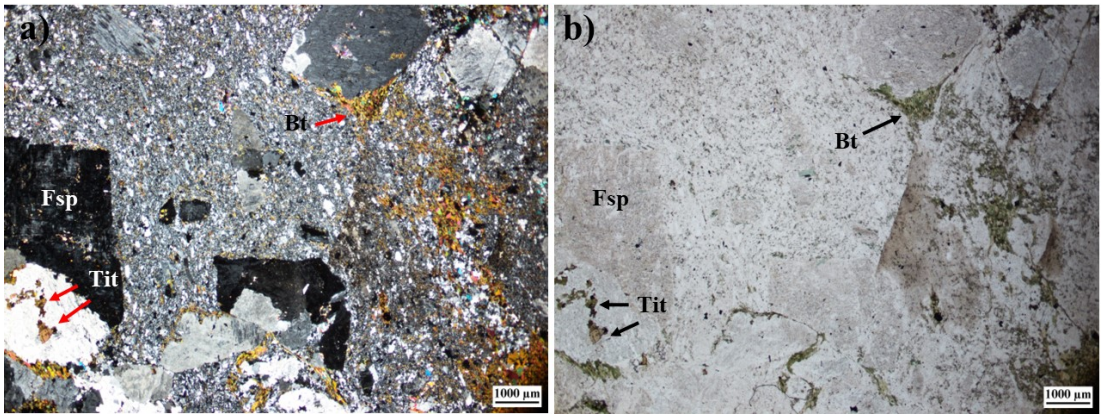

Fig. 19. Thin section of QP sample 124-1108 in cross polarized light (a) and plane polarized light (b). Glomerocrysts of feldspars, titanite, and biotite in a fine-grained groundmass abundant in quartz. Fsp = feldspar, Tit = titanite, Bt = biotite.

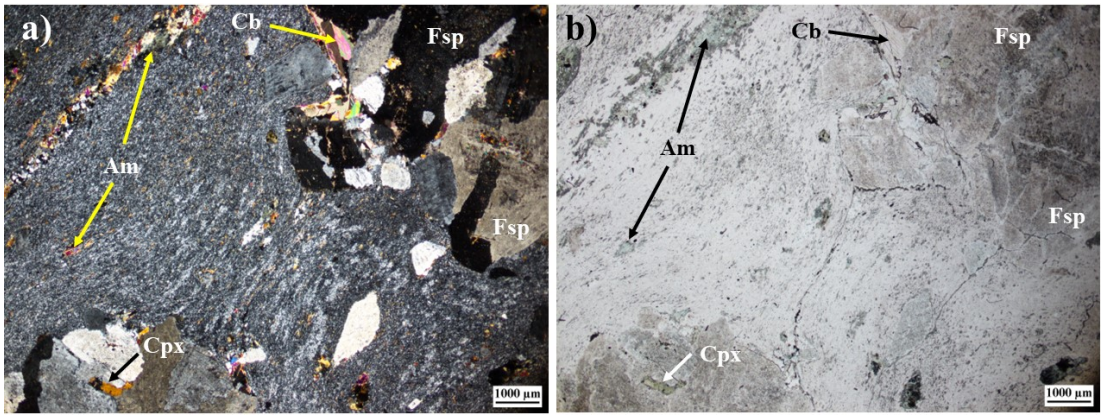

Fig. 20. Thin section of QP sample 335-1194 in cross polarized light (a) and plane polarized light (b). Glomerocrysts of feldspar, clinopyroxene, and carbonates. Amphibole and quartz in groundmass and as a veinlet in top right corner. Magmatic flow structure texture showing in groundmass. Fsp = feldspar, Cpx = clinopyroxene, Cb = carbonate, Am = amphibole.

Table 1. Petrographic observations. Am=Amphbole, Anh=Anhydrite, Bt=Biotite, Carb=Carbonates, Chl=Chlorite, Cpx=Clinopyroxene, Fsp=Feldspar, Gyp=Gypsum, Mag=Magnetite, Py=Pyrite, Qtz=Quartz, Tit=Titanite

Sample	Rock type	Colour description	Minerals and thin section observations *
84/1108	DP	Dark matrix, reddish glomerocrysts	Abundant green Bt, Anh, Chl, Am, Py, radioactive small minerals in Bt
139/1108 A	DP	Dark red matrix, white glomerocryst	Am, Anh, Carb, Flow structures
139/1108 C	DP	Dark green matrix, light glomerocrysts	Am, Cpx remnants in glomerocrysts, Anh, Carb, Flow structures
137/1137 B	DP	Reddish matrix, pink glomerocrysts	Bt, remnants of Am/Cpx, Carb, Anh, Flow structures
BG540	DP	Dark green matrix, white glomerocrysts	Am, Cpx-pseudo
215/1223	DP	Reddish greyish green matrix, reddish glomerocrysts	Cpx+Am, Flow structures
234/1137 B	DP	Greyish black matrix, dark glomerocrysts	Bt, Carb, Am
217/1137	DP	Red matrix, pink glomerocrysts	Cpx, some Am
215/1108	DP	Dark greenish grey matrix, light glomerocrysts	Am, Anh
205/1108 G	DP	Green matrix, light glomerocrysts	Cpx with Am-alterations, Carb
205/1108 R	DP	Red matrix, light glomerocrysts	Cpx with Am-alterations, some Anh and Carb, Flow structures
217/1079	DP	Greenish grey matrix, light pink glomerocrysts	Am, Anh, some Carb, Flow structures
318/1194 A	DP	Dark green matrix, reddish white glomerocrysts	Cpx, little to none Am
99/1108 A	DP	Dark green matrix, pink glomerocrysts	Am, abundant Anh/Carb
99/1108 B	DP	Dark greenish matrix, pink glomerocrysts	Am, remnants of Cpx, Am-needles, Anh, Carb
TG34/1338 R	DP	Reddish matrix, pink glomerocrysts	Am, Carb, Anh
TG34/1338 G	DP	Green matrix, light glomerocrysts	Am, Cpx remnants, some Carb, Flow structures
F2121/1223	DP	Reddish matrix, pink glomerocrysts	Cpx, some Am, Anh, Gyp, Flow structures
335/1194	QP	Reddish	Am, Cpx-pseudo and glomerocrysts, Carb
124/1108	QP	Dark greenish grey matrix, light glomerocrysts	Bt, Anh, some Mag, Flow structures
173/1165 B	QP/Ore	Red Qp	Complex contact Qp/Ore, Anh/Gyp in veinlets, larger Am in ore
178/1165	QP/Ore	Red Qp	Am, Am in veinlets, some Anh, some Mag, pseudomorphs after Cpx
*All samples contain Fsp glomerocrysts, Tit, Fsp and Qtz in matrix, Am-needles are common in most samples			

5.3 Geochemistry

The data of major and trace elements from both the LKAB reference data (21 838 analyses) and the present data set (18 analyses) have been screened to reduce the influence of contamination by ore and metasomatic alteration. Analyses with Fe_2O_3 greater than 10 wt% have been excluded to minimize the influence of iron ore, reducing the number of data to 17 688. Further, since large parts of the silicate country rocks to the ore in Kiirunavaara show alkali contents indicative of non-magmatic compositions, the 'igneous spectrum' of Hughes (1972) was applied to screen out the samples least affected by Na- or K-metasomatism (Fig. 21). The latter were subsequently used for further geochemical plotting and discussion (Fig. 23-27). This further reduced the LKAB reference data to a total of 4862 analyses: 148 DP, 3959 QP, and 738 SP.

Geochemical diagrams from Hughes (1972) and Montreuil et al. (2013) show that a large portion of the silicate rock mass associated with the Kiirunavaara ore is metasomatically altered, including the DPs, where a strong enrichment in Na dominates (Figs. 21 and 22). When using a major element classification diagram, plotting total alkalis versus silica, e.g., the TAS classification diagram from Le Maitre et al. (1989), a range in compositions from intermediate to rhyolitic is displayed for the dyke porphyries, overlapping with the compositions of both the footwall and hanging wall porphyries also after screening (Fig. 23). However, when applying the diagram after Pearce (1996), which is using trace elements considered more immobile during metasomatism, nearly all DPs plot in the rhyolitic fields, together with the QPs, while the SPs fall in the field of andesite/basaltic andesite (Fig. 24).

When it comes to alumina saturation of the Kiirunavaara rocks, including the DPs, a strong metaluminous dominance is observed, but with a minor subset of DPs and QPs being slightly enriched in aluminium (Fig. 25), while only very few QPs appear peralkaline. When using the Al_2O_3/TiO_2 vs Zr/Al_2O_3 diagram after Barrett et al. (2005), also using less mobile elements, a separation between the QP and SP is derived (some overlap may be due to misjudgement during logging), where the DPs again essentially overlap with the QP (Fig. 27).

Gorton & Schandl (2000) and Schandl & Gorton (2002) devised a tectonic discrimination diagram using Th/Yb versus Ta/Yb for felsic volcanic rocks associated with mineralizations, based on the diagrams of Pearce (1982, 1983). Plotting the Kiirunavaara data in this diagram shows a wide scatter, from within-plate volcanic zone to oceanic arc type compositions (Fig. 26). However, the 'centre of gravity' of the data is in the field of active continental margins, and most dyke porphyry samples analyzed in this study fall in this field.

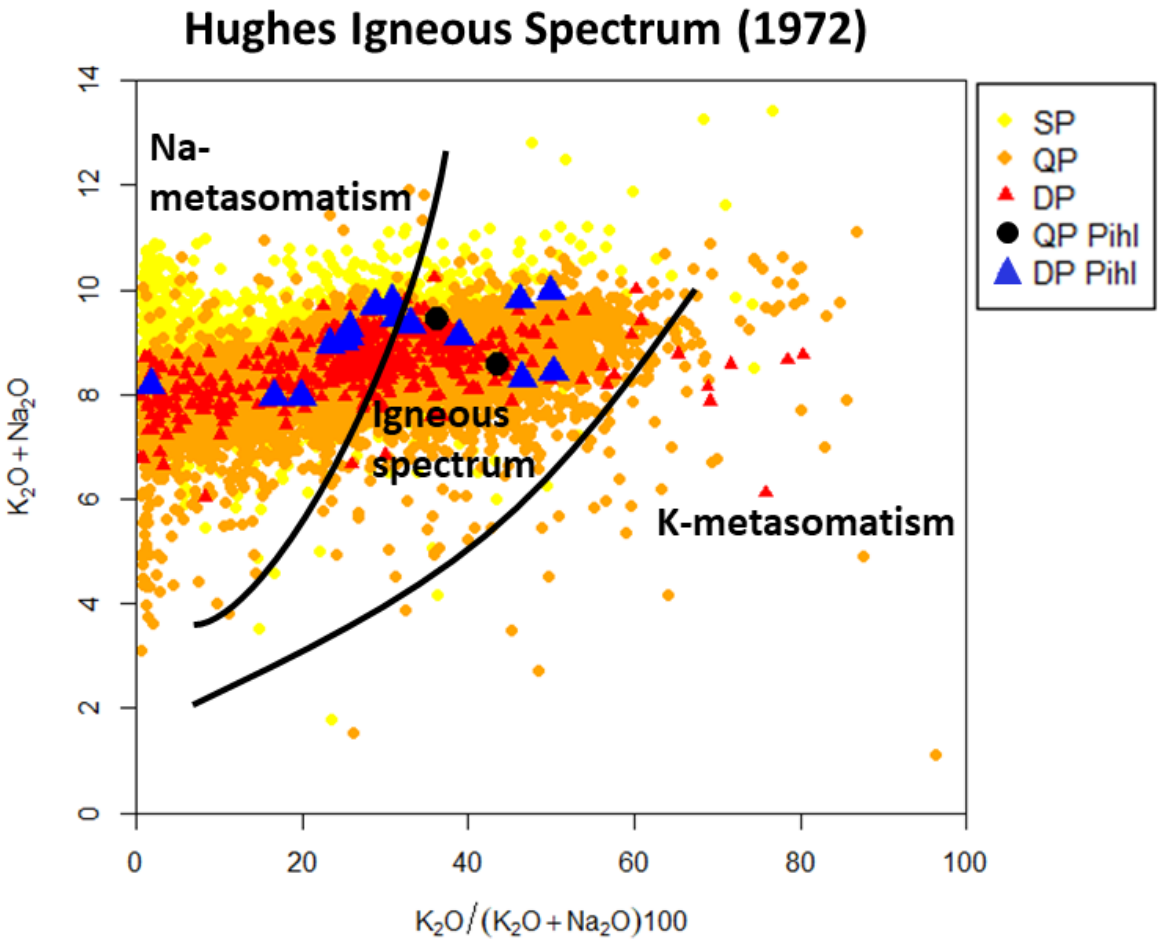

Fig. 21. Modified after Hughes igneous spectrum (1972). Igneous spectrum between the discrimination lines represents an unaltered magmatic composition. Strong alkali metasomatism, particularly Na-enrichment is observed. Samples marked "Pihl" from this study. The rest from the LKAB database.

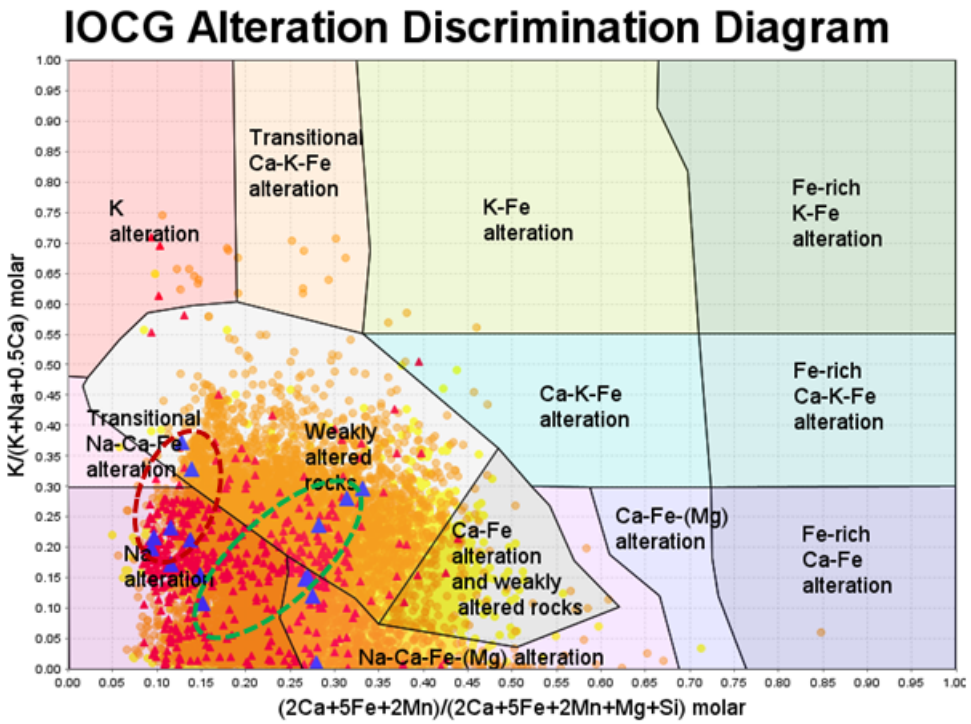

Fig. 22. IOCG alteration discrimination diagram after Montreuil et al (2013). Profound Na alteration trend, with some additional Ca-Fe alteration. DP Pihl data (blue triangles) inside dashed green lines are green samples and inside dashed dark red lines are red samples. *Legend as in Fig. 21.*

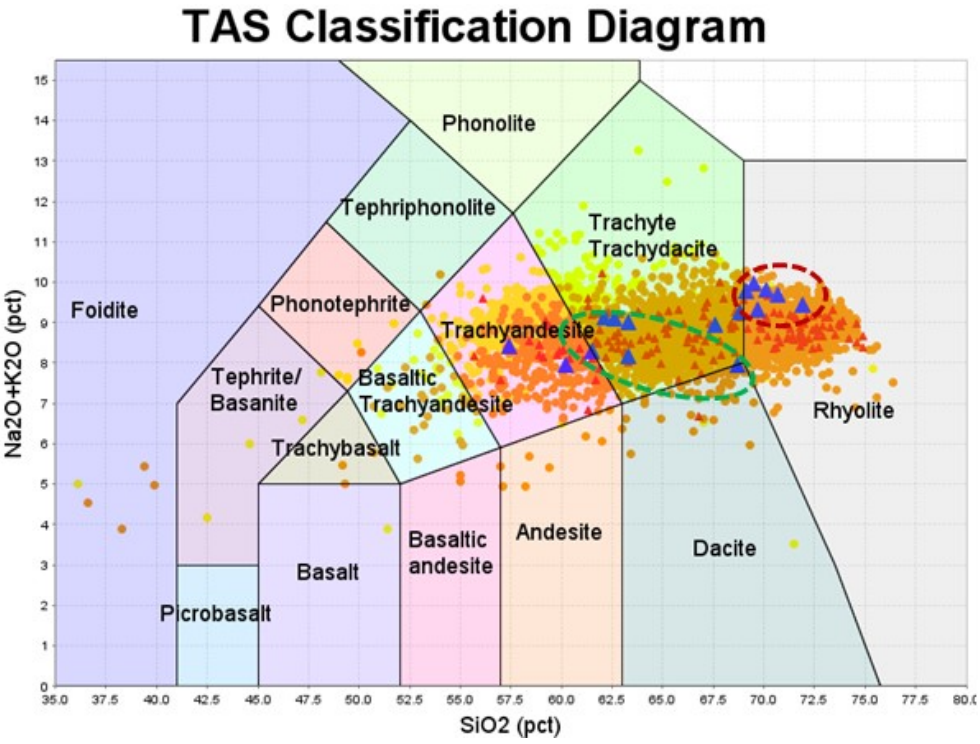

Fig. 23. Total alkalis versus silica after Le Maitre et al (1989). Dataset screened to within "igneous spectrum" in Fig. 21. Extensive overlap between all rock types. DP Pihl data (blue triangles) inside dashed green lines are green samples and inside dashed red lines are red samples. *Legend as in Fig. 21.*

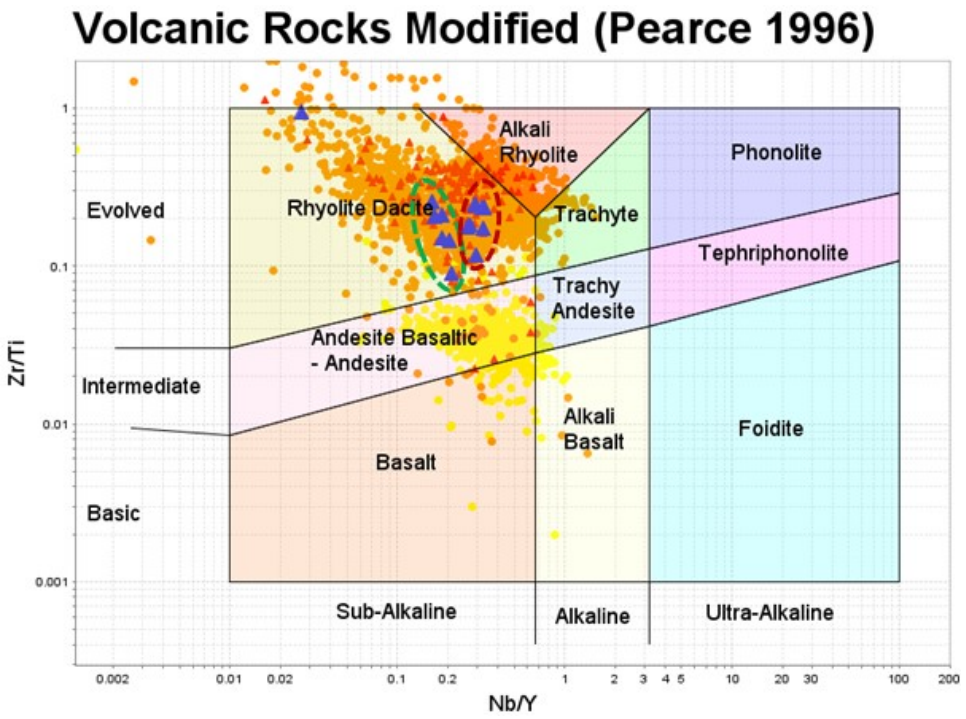

Fig. 24. Volcanic rocks diagram using 'immobile' trace elements, after Pearce (1996). Dataset screened to within "igneous spectrum" in Fig. 21. Clear separation between SP and QP. DP shows same composition as QP. DP Pihl data (blue triangles) of green samples plot inside green dashed lines and red samples plot inside dark red dashed lines. Dark DP samples plot more irregularly. *Legend as in Fig. 21.*

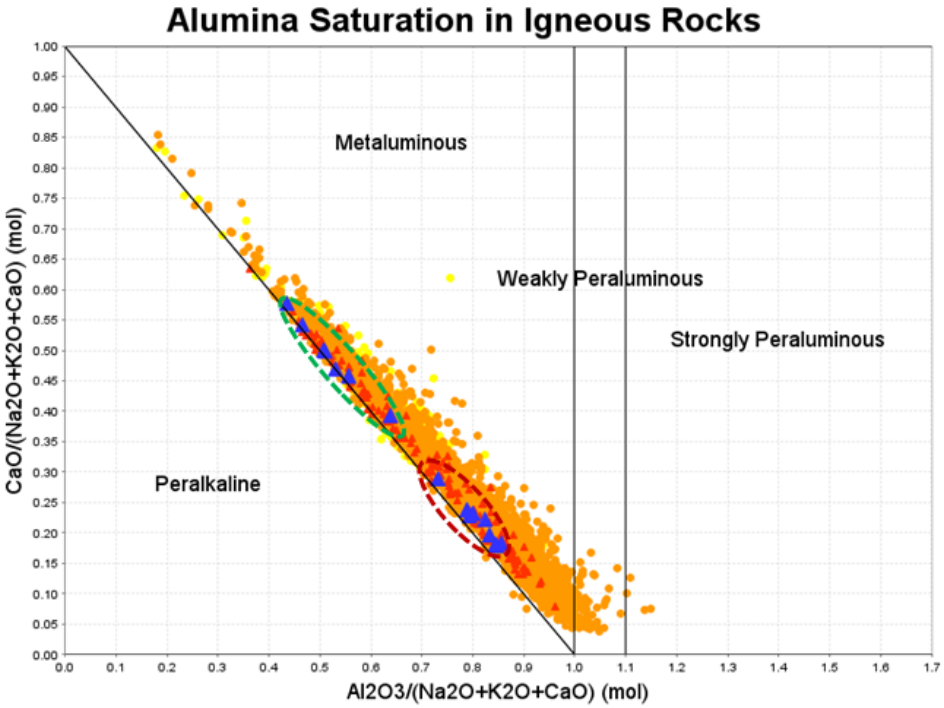

Fig. 25. Alumina saturation diagram after Barton & Young (2002). Dataset screened to within "igneous spectrum" in Fig. 21. Metaluminous compositions strongly dominant. A small number of QPs are

peraluminous and a very small number appear peralkaline. DP Pihl data (blue triangles) of green samples plot inside green dashed lines and red samples plot inside dark red dashed lines. Dark DP samples plot more irregularly. *Legend as in Fig. 21.*

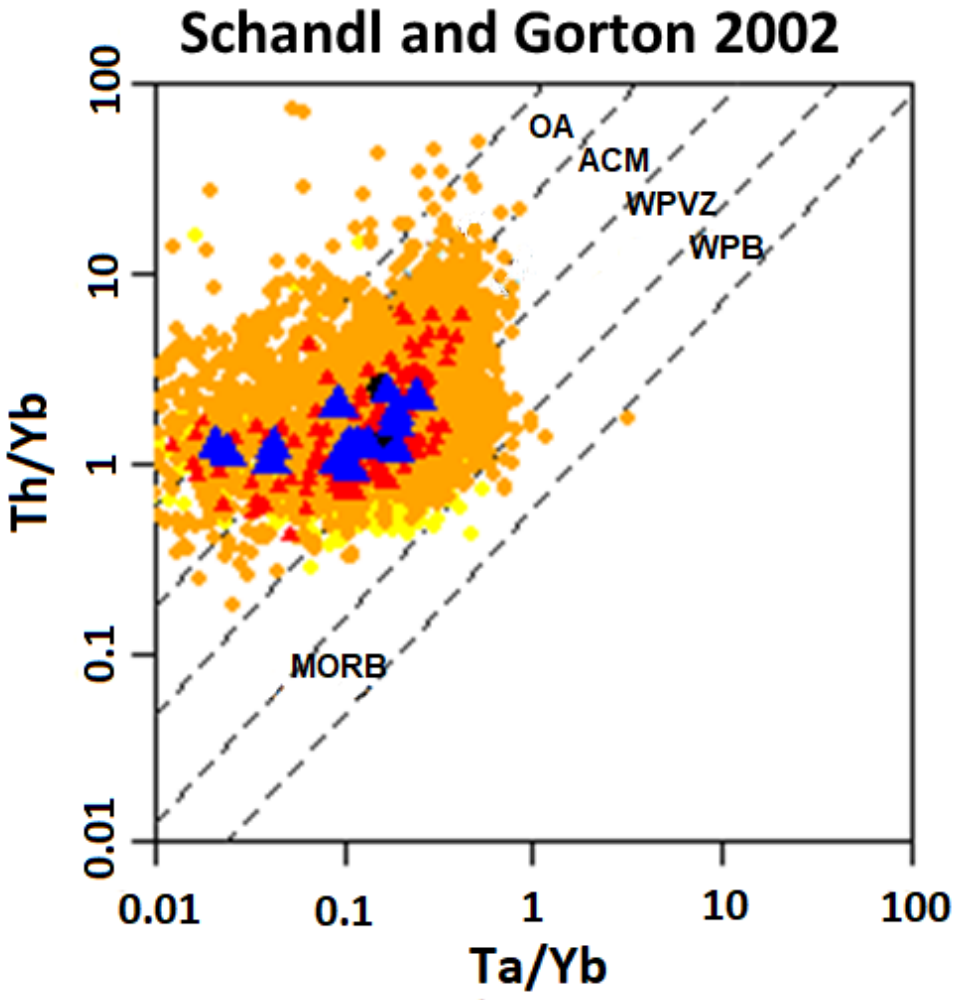

Fig. 26. Tectonic discrimination diagram using immobile elements Th/Yb v. Ta/Yb from Gorton & Schandl (2000), modified after Pearce (1982, 1983). Dataset screened to within "igneous spectrum" in Fig. 21. OA = Oceanic arc, ACM = Active continental margin, WPVZ = Within plate volcanic zone, WPB = Within plate basalt, MORB = Mid ocean ridge basalt. *Legend as in Fig. 21. Discussion in the text.*

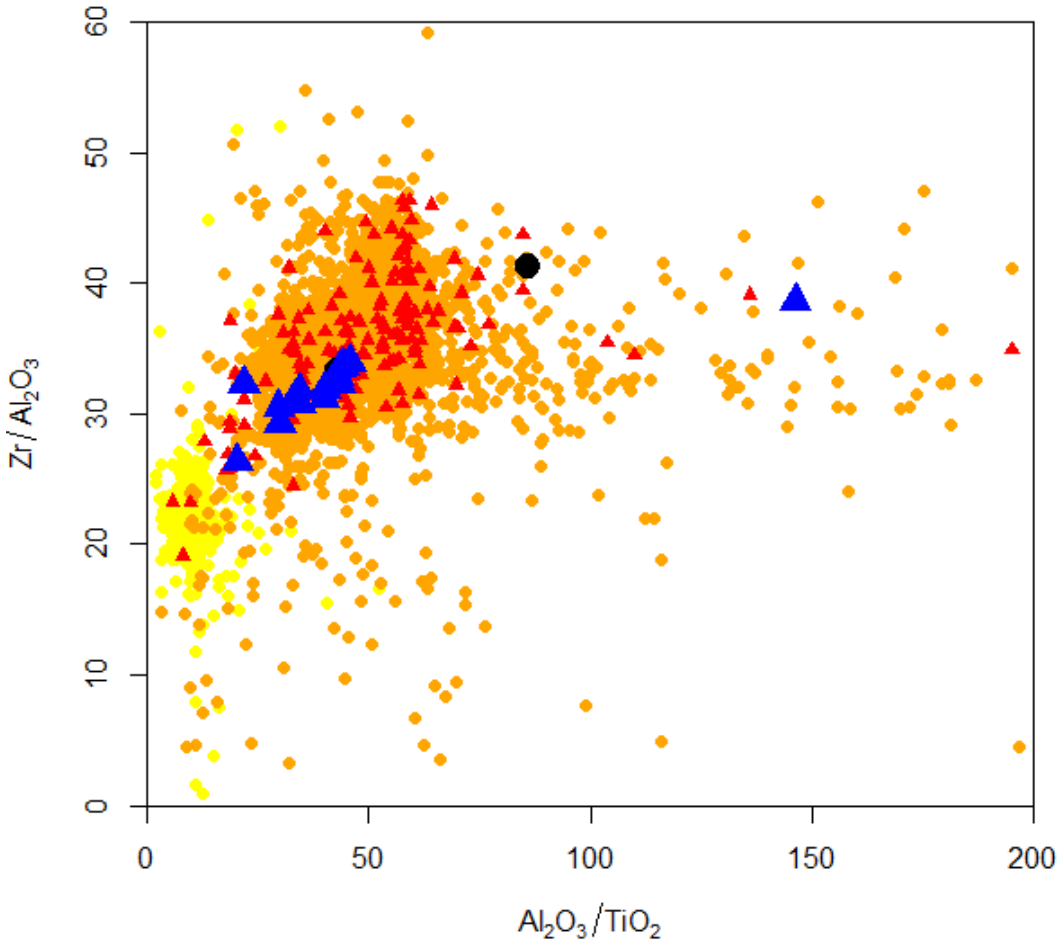

Fig. 27. Immobile elements ratio-ratio diagram of Al_2O_3/TiO_2 vs Zr/Al_2O_3 from Barrett et al (2005). Dataset screened to within "igneous spectrum" in Fig. 21. A fairly good separation between SP and QP is obtained, and the DPs overlap with the QP. *Legend as in Fig. 21.*

5.4 U-Pb geochronology

U-Pb age determination of dyke porphyry sample F2121/1223 was conducted for further understanding of the dykes role in the geological evolution of the Kiirunavaara area. Sample F2121/1223 indicated that the dyke porphyries are rich in zircon. Although most grains were too small to analyse with the LA-ICP-MS plasma beam diameter of 20 µm, 162 larger zircons suitable for the method were picked out.

Cathodoluminescence-imaging of the selected grains shows that the zircons range in size between 30 and 40 µm wide and between 50 and 150 µm long. The morphology of the zircon crystals was euhedral to subhedral (Fig. 28) Random fractures occur in most crystals but are not extensive and was avoided when analysed. The crystals show oscillatory zonation without indication of older cores, and a few have apatite mineral inclusions. No, or insignificant overgrowth textures were observed.

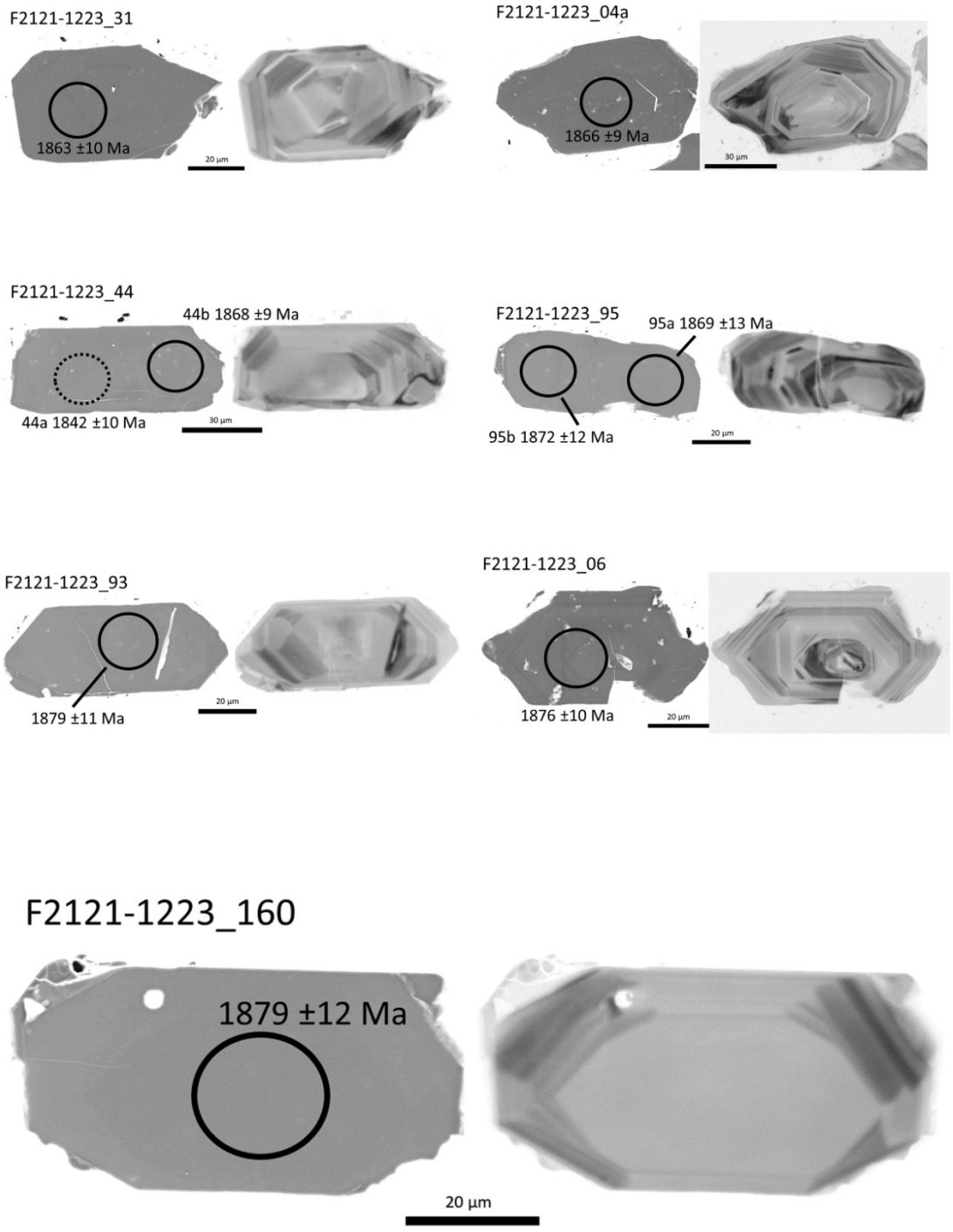

Fig. 28. Selected images of zircon grains representative for sample F2121-1223. BSE images on the left and CL images to the right. Circles show beam spot location of the LA-ICP-MS analyses and dashed circle is a discordant age. All ages are $^{207}Pb/^{206}Pb$ ages with uncertainties of 2σ.

40 analyses were conducted on 34 zircon crystals (Appendix III), of which 26 analyses yielded concordant results (Fig. 29). Only a few data points are discordant, or reversely discordant. All concordant, within error overlapping analyses yielded a U-Pb concordia age of 1880 ± 4 Ma, which is considered to represent the crystallization age of the sample. A weighted mean 207Pb/206Pb age of all within error overlapping concordant and near concordant data yielded 1878 ± 4.8 Ma (Fig. 30). A couple data points lie above the concordia to the left with relatively large errors, while three analyses lie outside the errors of those in the age calculation, but concordant closely to the left. None of these can be correlated with any aberrant zoning and may therefore represent some ancient change in Pb composition or analytical problems.

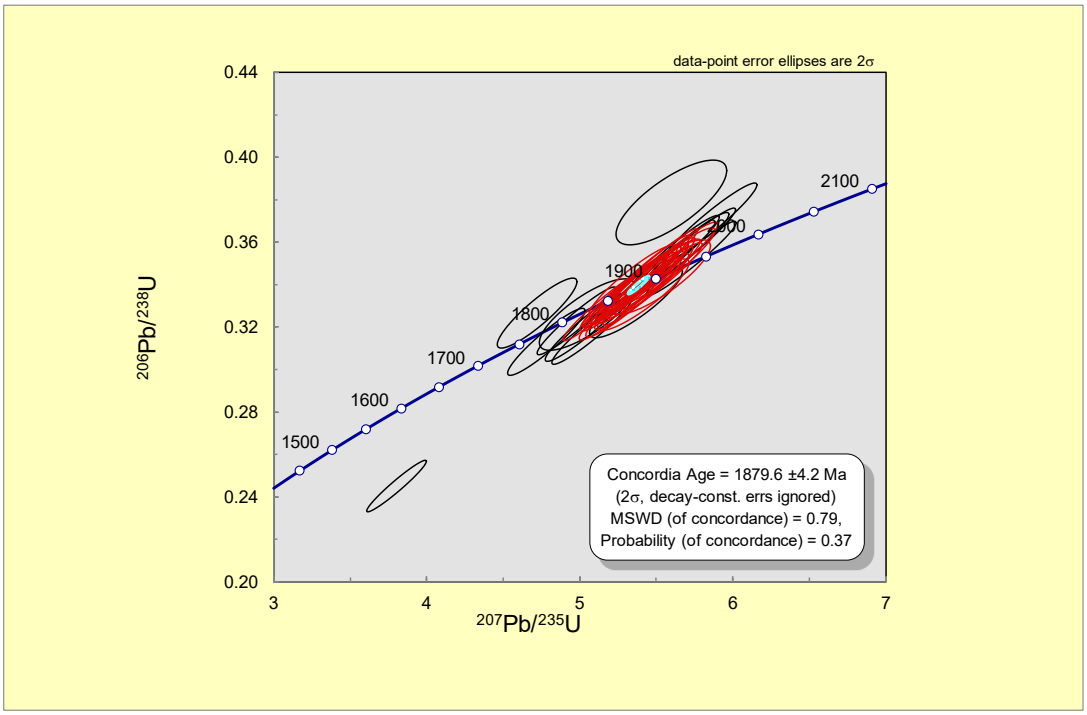

Fig. 29. Concordia diagram of analyzed spots in zircon crystals from sample F2121 1223. Light blue ellipse represents the concordia age 1879.6 ±4.2 Ma and red ellipses are all the concordant analyses.

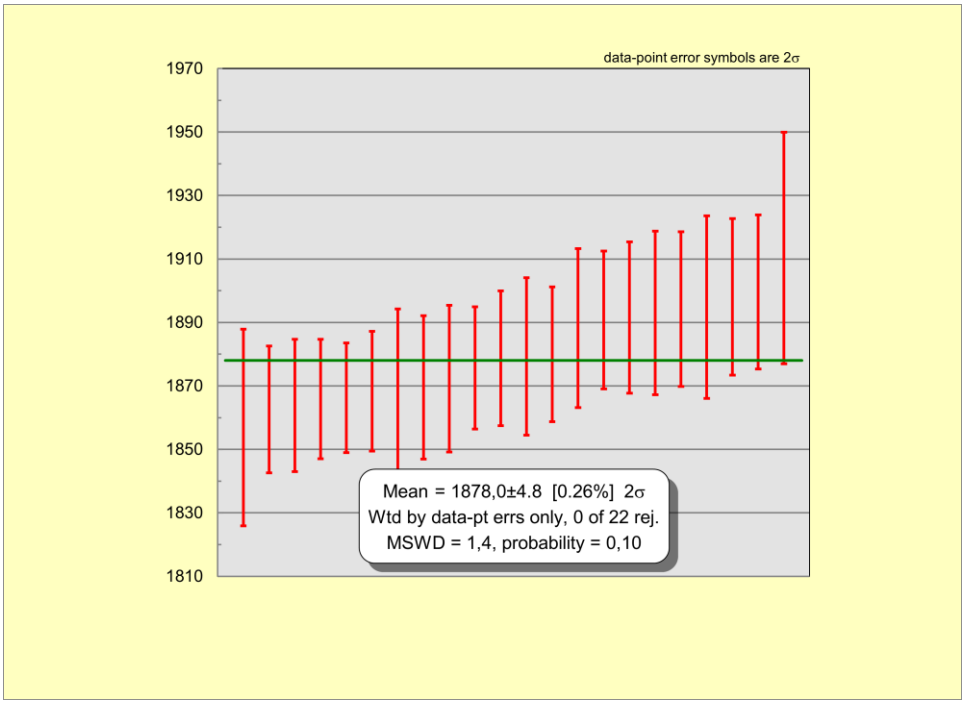

Fig. 30. Weighted mean age of all analyses with overlapping ages from sample F2121 1223, 1878 ± 4.8 Ma.

6 DISCUSSION

Texture

Field observations show the porphyritic texture of the DPs with rounded anhedral to almost euhedral feldspar phenocrysts/glomerocrysts in an aphanitic groundmass to be essentially identical with the one observed in the hanging wall QPs (cf. Figs. 7, 8, and 10). Size, shape, colour, and distribution density of the phenocrysts, as well as groundmass characterizations, vary slightly between samples but stay more or less consistent between the two, as noted also by Geijer (1919) and Sandberg (2018). This makes them visually inseparable. Conspicuous for the dyke porphyries are their common green or red colour variations of the groundmass (Fig. 7) whereas the quartz-bearing porphyries more typically are red to dark grey but green varieties also occur.

Petrographic observations of thin sections along with sample descriptions from this study show the dyke porphyries to be texturally inseparable from the hanging wall quartz-bearing porphyries even at microscopic scale. Additionally, their mineralogical characteristics match up altogether without major inconsistencies. The main mineralogical composition is feldspar

glomerocrysts, typically associated with large clinopyroxene, amphibole, and titanite, in an aphanitic groundmass. The latter is abundant in feldspar and quartz, with the green silicates clinopyroxene and amphibole in cases occupying c. one third of the groundmass, which corroborates observations of Geijer (1910) and reference material from Sandberg (2018) used in this thesis. Dyke porphyry samples of Sandberg (2018) did not, however, contain any biotite, contrary to what have been observed in this study; in a few samples and mentioned earlier by Geijer (1910). Samples rich in biotite, both in dyke porphyries and quartz-bearing porphyry, are almost completely lacking clinopyroxene and amphibole, which seem to have been replaced by the biotite. Further, Sandberg (2018) concludes that the dyke porphyries contain less quartz but more clinopyroxene than the quartz-bearing porphyries. This corresponds to the green dyke porphyry samples from this study, but not with the red-coloured samples. Magmatic flow structures in the groundmass are common in most samples, both DP and QP, as well as some signs of pressure shadows around phenocrysts aligning mineral grains in the direction of flow/foliation, as previously noted also by Geijer (1910), Ekström & Ekström (1977), Berglund et al. (2010), and Sandberg (2018). Groundmass colour variations are here described for the green samples as abundant clinopyroxene and/or amphibole in the matrix and in the red samples as staining by iron oxide alteration in the fine-grained feldspar matrix (Fig. 18). Whichever of these are the prominent in the samples seem to be what gives the final colour to it. More reasoning and detailed cause of this opens for further research. The darker colour variations represent samples where the green silicates have been replaced by biotite.

Field observations

The dyke porphyries of Kiirunavaara, irregularly winding through the ore body and its footwall host rock, can be observed to cut through its surroundings at a high angle but also spreading out along direction of the stratigraphic layering, inside both the footwall, ore body, and at their contacts (Fig. 5). In detail, contacts are typically sharp but irregular. As the dyke porphyries reach the hanging wall, they seem to disappear merging with the HW porphyries without distinguishable contacts separating them (cf. Geijer, 1960), which is to be expected given their inseparable texture and overprinting geochemical character.

Observations of the porphyry dykes forming rounded enclaves in ore, in a fashion similar to co-mingling of magmas, have been observed in several places (Figs. 3 and 12). Similar relations are also observed between the ore and HW rocks along the contact (Fig. 12B), as well as ore enclaves within the HW porphyries further away from the ore (Geijer, 1968; Andersson, 2013). Sample 173/1165B (Fig. 10) from QP/ore contact show mingling structures also between hanging wall and ore.

These contact relations indicate a close to coeval existence of pulses of dyke porphyry magmas with the emplacement of ore magma, as previously discussed by Geijer (1910, 1919, 1960) and Andersson (2013). The latter further discusses the magma mingling structures observed to indicate contemporaneous activity of the magmas in a model of coeval eruption, as well as interpreted the dyke porphyries as feeder channels for at least part of the hanging wall volcanism (a possibility also discussed, but dismissed, by Geijer 1919), also explaining the occurrence of footwall and ore enclaves in the hanging wall. Observations and results from this study give further grounds for advocating this to be the case (see also Andersson et al. 2024).

Geochronology

Results of the zircon analysis show euhedral zircons with typically magmatic oscillatory zonation without indications of older cores. A few showing apparent younger ages may be the result of ancient lead loss or analytical problems. The concordia age obtained in this study at 1880±4 Ma is considered as the best estimate of the crystallization age of the dyke porphyry. The weighted average $^{207}Pb/^{206}Pb$ age (1878 ± 4.8 Ma) coincides with the concordia age within error.

This age falls within errors of the range of previous studies for the Kiruna IOA ores and host rocks (Romer et al., 1994; Westhues et al., 2016; Billström et al., 2019). Westhues et al. (2016) presented concordia ages at 1874 ± 7 Ma for the ore, 1877 ± 12 Ma for the footwall syenite porphyry, and 1880 ± 7 Ma and 1880 ± 4 Ma for the hanging wall quartz-bearing porphyry. The overlapping crystallization ages of the IOA ore and host rocks, including the crosscutting dyke porphyries, support the closeness in time of the magmatic activity, and is not at variance with models of more or less synchronous magmas.

Geochemistry

Geochemically, the dyke porphyries and the host rocks to the ores in Kiirunavaara are strongly enriched in Na, having been metasomatically altered (Figs. 21 and 22). This complicates interpretations of magmatic compositions as the result shows the present-day constituents of the rocks, rather than the primary, unaltered rock. Therefore, data screening removing samples with high iron (Fe_2O_3 > 10 wt%) as well as samples outside Hughes (1972) ‘igneous spectrum’ was necessary to filter out data as unaltered as possible.

The dyke porphyry data of this study, LKAB reference data of dyke porphyry and quartz-bearing porphyry are geochemically inseparable and completely overlap each other (cf. all geochemical plots). The footwall syenite porphyries differ slightly from these by plotting more towards the intermediate compositions, even though overlaps are large. Major element classification diagrams (Le Maitre et al., 1989) show a wide range in compositions for the dyke porphyries from trachyandesitic intermediate to rhyolitic composition. However, in immobile trace element diagrams (Figs. 24 and 27) there is a separation of DP/QP into rhyolite-dacite fields and SP into andesite fields (Fig. 24). Thus, the essentially immobile trace element ratio diagrams are able to, at least partly, 'see through' the alteration and separate the ore-associated silicate rocks into two groups, while the major element compositions are still affected by the alkali metasomatism also in samples screened into the "igneous spectrum". Interestingly, the 'younger' DPs show the same metasomatic trend as the QPs.

The present (DP Pihl) dyke porphyry geochemical analysis results in the IOCG alteration discrimination diagram, the TAS classification diagram, volcanic rocks diagram, and alumina saturation diagram can be distinguished into two groups (Fig. 22-25), as the red samples on the whole separate from the green samples, with dark samples occurring more irregularly. Figures of geochemical diagrams without dashed circles (Fig. 21, 26, and 27) plot the DP data more scattered, and therefore, separation between red and green samples was not possible. TAS classification diagram plot the red samples in the rhyolite field whereas most green samples plot in the trychyte-trachydacite field. Green and dark samples also plot more, although not exclusively, outside the 'igneous spectrum' (Hughes 1972) than the red samples, indicating the green and dark samples to be more heavily altered than the red samples. Hanging wall hydrothermal alteration discussed by Paolillo & Giapis (2021) and Lupoli et al. (2022) supports pervasive sodic alteration of the silicate rocks of Kiirunavaara, with Na-Ca alteration proximal to the ore, transitioning via Ca-Fe alteration to a distal K-Fe alteration (Paolillo & Giapis, 2021), but with a possible later potassic event overprinting and partly replacing actinolite (Lupoli et al., 2022). Dyke porphyry results of this study can be included here, as the geochemistry shows extensive Na-metasomatism and indications of Ca-Fe alteration. Red dyke porphyry samples appear to represent a more Na-, Na-Ca-dominated alteration, while green samples in contrast trend more towards the Na-Ca-Fe and Ca-Fe alteration character (Fig. 22). Moreover, the dark biotite samples would represent a possible later potassic event overprinting an earlier calcic alteration discussed by Lupoli et al. (2022). In depth discussion of the reasons and age of the metasomatism is outside the scope of this study.

Most of the volcanic and dyke porphyries are metaluminous, only a minor subset of QP/DPs are peraluminous. Assuming this was the case also before metasomatism, the sources of these volcanics should be metaigneous rather than metasedimentary (e.g., Chappell & Stephens

1988; Scaillet et al., 2016). In the diagram by Schandl and Gorton (2002), for tectonic environments, using the Ta/Yb versus Th/Yb diagram, most of the dyke porphyries plot in the field indicating active continental margin environments, with a few analyses falling into the field indicating oceanic arc. Hanging wall quartz-bearing porphyry and footwall syenite porphyry plot in a wider range from within-plate volcanic zone to oceanic arc, but still a large majority fall in arc fields, supporting previous suggestions of continental arc settings for this group of volcanics (e.g. Martinsson et al., 2016; Sarlus et al., 2020; Andersson et al., 2021).

Considering the dyke porphyries as feeders of the hanging wall volcanism this division of DPs could be interpreted as different generations or pulses of dyke porphyry magma.

7 CONCLUSIONS

The dyke porphyries of Kiirunavaara have been exposed to an extensive Na-metasomatic alteration, as is also the case for other silicate rocks associated with the IOA ore. Two distinct colour variations typical for the dyke porphyries constitute a red variety caused by staining of iron oxide alteration in feldspars of the fine-grained matrix, and a green variety due to abundant fine-grained green clinopyroxene and amphibole in the matrix. A third, less evident, dark variety implicates replacement of the green silicates by biotite. The difference in geochemistry between the green and red dykes suggests that they may represent two separate magma pulses. The obtained U-Pb concordia age of 1880±4 Ma for a sample of dyke porphyry overlaps within error all other rocks of the Kiirunavaara group and shows that these dykes are an integral part of the volcanic history. Geochemically the dyke porphyries completely overplot the hanging wall quartz-bearing porphyries, with which they also share conspicuously similar textural characteristics. They form irregular dykes, transecting both the footwall volcanics and ore, merging into the hanging wall volcanics without visible contacts.

Considering all the above, this study concludes that the dyke porphyries represent magmas of identical compositions as the hanging wall volcanics and most probably were feeder channels for the hanging wall volcanism. The intrusions of dyke porphyry magmas occurred in pulses in an active continental margin environment, at the waning stage of footwall and ore magmatism, generating both crosscutting and mingling relations with the ore body.

ACKNOWLEDGEMENTS

First and foremost, I want to thank my supervisor Ulf B Anderson at LKAB for giving me the opportunity for this master's thesis project, for all his support and patience. Also, I want to thank my supervisor Olav Eklund at Åbo Akademi University for his guidance along the way.

I want to thank Alpar Kovacs for providing geochemical reference data from the LKAB database, Matti Kurhila at the Geological Survey of Finland (GTK) for his supervision with LA-ICP-MS U-Pb age determination and data processing, Sören Fröjdö (Åbo Akademi University) for his guidance and help with geochemical data screening, Arto Peltola (University of Turku) for producing thin sections, and Ermei Mäkilä (University of Turku) for CL-imaging opportunity. I would also like to thank all my colleagues (and former colleagues) at LKAB for their support and showing interest in this project, especially Henrikki Rutanen for helping send samples to ALS laboratory, Etienne Lindborg Bordenave for collecting samples, Lizet Fonseca and Ann Bäckström for the help with Leapfrog Geo visualization, and Sergio Castro Reino for all the interesting discussions.

Finally, thank you to all my friends and family for the endless support during all these years.

SUMMARY IN SWEDISH – SAMMANFATTNING PÅ SVENSKA

Gångporfyrerna i Kiirunavaara – geologi, geokemi och mineralogi

Introduktion

Kiirunavaara, som är känt för sin apatitjärnmalm, är beläget i norra Norrbotten som en del av den Fennoskandiska skölden (e.g.,Martinsson et al. 2016). Apatitjärnmalmens angränsande gråberg består av ett antal olika bergarter, däribland gångporfyrerna. Gångporfyr är en finkornig, porfyrisk bergart som på ett oregelbundet vis genomskär liggväggsbergarterna syenitporfyr och själva malmkroppen men sedan försvinner in i hängväggens kvartsbärande porfyrer (Geijer 1910; 1960; Andersson 2013).

Den tidigaste beskrivningen av gångporfyrerna är från Geijer (1910) och efter detta har de diskuterats begränsat. Här ligger fokus på gångporfyrerna och syftet är att beskriva mineralogiska och geokemiska karaktärsdrag, samt geologisk ställning och ålder. Slutsatser baserat på detta kan ge ytterligare information om gångporfyrernas uppkomst och roll i den geologiska utvecklingen relaterat till Kiruna-typens malmbildning.

Texturmässigt är gångporfyrerna väldigt lika, näst intill omöjliga att skilja från hängväggens kvartsförande porfyrer. Tidigare forskning tyder på att gångporfyrerna kan ha fungerat som tillförselkanaler för hängväggsvulkanismen (Geijer 1919; Andersson 2013) vilket prövas här med ytterligare data.

För den här avhandlingen har prover av gångporfyr och kvartsförande porfyr från Kiirunavaara gruva samlats in för att utföra analyser mineralogiskt i optiskt mikroskop, geokemiska analyser av huvud- och spårelement samt en U-Pb åldersdatering av zirkon i ett prov gångporfyr.

Geologisk bakgrund

Den regionala geologin i Norrbotten består av en underliggande arkeisk berggrund, 2.8–2.6 Ga, överlagrad av proterozoiska bergartssekvenser: de Karelska, 2.5–2.0 Ga, och Svekofenniska, 2.0–1.8 Ga, samt intrusioner av enorma magmatiska sviter 2.0–1.8 Ga (Bergman & Weihed 2020). Dessa uppdelas stratigrafiskt i den karelska Kovogruppen (2.5–2.3 Ga) och Kirunagrönstenarna (2.3–2.0 Ga), samt de svekofenniska: Kurravaarakonglomerat, Kiirunavaaragruppen och Haukigruppen (Martinsson 1997; 2004; Bergman & Weihed 2020). Apatitjärnmalmerna i Kirunaområdet uppträder i Kiirunavaaragruppens bergarter (Martinsson et al. 2016, 2004; Bergman & Weihed 2020), som ytterligare delas in i formationerna Hopukka, Luossavaara och Matojärvi (Martinsson, 2004). Här domineras berggrunden av lågmetamorfa trakyandesitiska lavaflöden och porfyrisk ryodacit (Geijer, 1910).

I norra Norrbotten finns cirka 40 kända fyndigheter av apatitjärnmalm (Martinsson et al 2016). Kiirunavaara är den största av dessa med uppskattade >2 000 Mt malm före brytning (Martinsson 2004) och brytning bedrivs i dagsläget av LKAB (Kiirunavaara Luossavaara Aktiebolag).

Variationer i apatitjärnmalmen finns mellan de olika fyndigheterna som uppvisar variationer i järnhalt på 30–70 % och fosforhalt 0.05–5 % (Niiranen 2006; Bergman et al. 2001). Järnmalmen kan uppdelas i en breccierad typ och en ”stratiform-stratabunden” typ, beroende på dess uppträdande och associerade omvandlingar och gråberg (Martinsson et al. 2016).

Sedan sent 1800-tal (e.g., Löfstrand 1891; Geijer 1910b) har järnmalmens uppkomst och de malmbildande processerna debatterats och fortfarande saknas en enande modell (cf. e.g., Parák 1975a; Frietsch 1984; Nyström 1985; Hitzman et al. 1992; Smith et al. 2009; Andersson 2013; Troll et al. 2019). Geijer (1910a) talar för en magmatisk modell och malmbildning ur differentierade järnoxidmagmor. Parák (1975b) däremot föreslår ett vulkanisk-exhalativt system. Westhues et al. (2016; 2017) hänvisar till hydrothermala vätskor från närliggande

intrusioner, och andra förespråkar en magmatisk/magmatisk-hydrotermal modell (Nyström et al. 2008; Troll et al. 2019).

Liggväggsbergarterna i Kiirunavaara är en del av Hopukka-formationen (Martinsson, 2004) och består av ett flertal trachyandesitiska lavaflöden och intrusiva bergarter (Geijer 1960, Bergman et al 2001; Westhues et al. 2016). Geijer (1910a) kallar liggväggens trakyandesiter för syenitporfyrer (SP), vilket också används inom gruvan. Han beskriver variationer i sammansättning och texturer från en medelkorning syenit uppåt mot en finkornig syenitporfyr. Även en variant av SP kallad mandelporfyr beskrivs. Syenitporfyrerna består av ett afanitisk matrix dominerat av fältspater tillsammans med amfibol, magnetit och titanit (Geijer 1910; Sandberg 2018). Ljusa fältspatfenokrister som är 1–3 mm stora är vanliga i syenitporfyren. Mandelporfyen består av mörka noduler av amfibol, titanit, magnetit, apatit, och glimmer, vanligen under 1 cm i storlek (Geijer 1910a, Palm 2015; Gray 2016). Andersson (2013) finner mandelporfyren speciellt förekommande i närheten av malmen. Syenitporfyren är fattig på zirkon men har U-Pb-daterats via ett $^{207}Pb/^{206}Pb$ viktat medelvärde till 1884 ± 4 Ma och med en konkordiaålder om 1877 ± 12 Ma (Westhues et al. 2016).

Hängväggsbergarten är en del av den Hopukka överliggande Luossavaara-formationen och är en ca. 800 m mäktig succession av vulkaniska porfyrer (Martinsson et al. 2016). Enheten består av en mängd eruptiva lager med enklaver härstammande från stratigrafiskt lägre lager (Geijer 1968). Sammansättningen är ryodacitisk och tolkad bestå främst av pyroklastiska flöden som innehåller rikligt med 2–5 mm stora fältspat fenokrister/glomerokrister (e.g., Ekström & Ekström 1997; Martinsson et al. 2016; Sandberg 2018). Ryodaciterna beskrivs av Geijer (1910) som kvartsporfyrer p.g.a. den afanitiska grundmassan av fältspat och kvarts, trots ofta frånvarande kvartsfenokrister. Senare ändrade han namnet till kvartsförande porfyrer (Geijer 1931) och i gruvan förkortas de som QP. Övriga mineral som förekommer är bland annat amfibol, magnetit, titanit, biotit och apatit (Geijer 1910a; Berglund et al. 2010; Sandberg 2018). Zirkoner förekommer rikligt i de kvartsförande porfyrerna och har U-Pb daterats till konkordiaåldrarna 1879.5 ± 7.1 Ma och 1880.5 ± 4.5 Ma (Westhues et al. 2016).

Gångporfyrerna nämns först av Geijer (1910a) som syenitporfyrgångar inom liggväggen men senare (Geijer 1960) benämns de som gångporfyrer. Gångporfyrerna uppträder i liggväggen och malmen som gångar i öst–västlig riktning men breder också ut sig i nord–sydlig riktning längs de stratigrafiska lagren. Gångarna har observerats genomskära malmen men också vara uppsprucken av den vilket tyder på intrusioner av gångporfyr både före och efter malmuppkomst (Geijer 1910, 1919, 1960). Andersson (2013) diskuterar samtidig aktivitet av magmorna vilket förklarar strukturer av magmablandning (’magma mingling’). Gångporfyrerna består av rundade fältspatfenokrister och glomerokrister i ett afanitiskt matrix

dominerat av fältspat, men även kvarts, amfibol och pyroxen. Accessoriska mineral är apatit, magnetit och titanit (Geijer 1910a, Sandberg 2018). Gångporfyrerna är till texturen näst intill identiska med de kvartsbärande porfyrerna i hängväggen, där gångarna verkar försvinna utan observerade kontakter.

Material och metoder

Från Kiirunavaara gruva har provtagning av gångporfyr gjorts på 14 lokaler och av kvartsförande porfyr på 4 lokaler. Från de insamlade proven har det gjorts tunnslip, geokemiska analyser och en åldersdatering. Resultat från denna avhandling har jämförts mot tillgängligt referensmaterial från LKAB:s databas i form av totalt 21 838 geokemiska analyser av relevanta bergarter och tunnslip från Lindgren (2013) och Sandberg (2018).

Provberedning gjordes av prov från samtliga lokaler till 22 tunnslip. Krossat och malt prov skickades till ALS laboratorier för geokemisk analys och zirkoner för geokronologi togs fram genom en mineralsepareringsprocess.

Åldersdatering med U-Pb-metoden bygger på sönderfall av de radioaktiva isotoperna av uran till deras stabila dotterisotoper av bly, ^{238}U till ^{206}Pb och ^{235}U till ^{207}Pb. Mineralet zirkon används ofta för denna metod då det är ett vanligt förekommande mineral i jordskorpan och besitter fysikaliska och kemiska egenskaper lämpliga för att motstå extrema förhållanden (till exempel, Hanchar, 2003; Harley & Kelly 2007). Analys utfördes med metoden LA-ICP-MS (Laserablation, induktivt kopplad plasmamasspektrometri) där provet med zirkoner förs in i en ablationscell där det blandas med helium och argongas och det abladerade materialet bildar ett plasma och sedan förs in i spektrometern för analys. Kalibrering och standardprov kördes med jämna mellanrum och efteråt korrigerades rådatan i programmet Glitter (Van Achterbergh et al, 2001) för bakgrundsstrålning, massdiskriminering och laserinducerad grundämnesfraktionering.

Geokemianalyser utfördes på huvud- och spårelement hos ALS laboratorier med deras respektive metoder ME-ICP06 och ME-MS81. Huvudelementen bryts ner via litiumborat- och syraupplösning för att frigöra elementen som sedan analyseras av ett ICP-AES-instrument (Optisk emissionspektrometri med induktivt kopplad plasma) där grundämnen urskiljs enligt deras olika karakteristiska våglängder av ljus de avger. Spårelementen analyseras i sin tur av en ICP-MS (induktivt kopplad masspektrometri) där plasman frigör grundämnen i provet till joner som sedan separeras enligt deras förhållande mellan massa och laddning (ALS, 2023).

Resultat

Gångporfyrerna i Kiirunavaara uppträder som oregelbundna, genomskärande gångar upp till 10 meter breda i liggväggen och malmkroppen. Geologiska modeller visar en koncentration av gångporfyrer i de centrala delarna av gruvan. De uppträder i rummet i öst-västlig, samt nord-sydlig riktning spridda längs med malm-liggväggskontakten. Gångarna i liggväggen begränsas ofta av skarpa oregelbundna kontakter, medan de i malmen kan var ”breccierade” eller ”minglade”. Gröna och röda varianter av gångporfyr är vanliga men också mörka/gråa varianter förekommer. Texturen är porfyrisk med ljusa/ljusröda fenokrister i den afanitiska grundmassan. Hängväggens kvartsbärande porfyrer är till texturen identiska med gångporfyrerna. De är ofta röda eller mörka till färgen och visar mindre variationer jämfört med syenitporfyrerna i liggväggen.

Petrografiska observationer av tunnslip på gångporfyrerna utfördes med optiska mikroskop. Fältspatfenokristerna är ljusa till ljusröda, några millimeter till centimeter stora kristaller anhopade till glomerokrister, vanligen tillsammans med klinopyroxen, amfibol och titanit. Fältspaterna visar diffusa sammanväxningar av kalifältspat och plagioklas med mikroklina texturer tillsammans i ett pertitiskt mönster med albit, som ibland uppvisar tvillingbildning. Grundmassan är även huvudsakligen sammansatt av fältspat, ofta tillsammans med rikligt av kvarts.

För övrigt består gångporfyrerna till stor del av klinopyroxen och amfibol i glomerokrysterna eller som en del av grundmassan. Klinopyroxenerna uppträder som bruna blockiga korn, ofta delvis omvandlade till, eller ersatta av, amfibol. Amfibolerna är gröna oregelbundna korn men uppträder också som små nålar i fenokrister eller grundmassan. Titanit är vanligt förekommande i alla prov bland fenokrister och i mellanmassan.

Andra mineral som förekommer är kvarts i grundmassan eller större korn i aggregat intill glomerokrister. Aggregat av karbonater, mest troligt kalcit, är typiskt i de flesta prov. Sliror av grön biotit förekommer i en del prov och i ett av dem med radioaktiva mineralinneslutningar. Anhydrit förekommer ofta tillsammans med aggregat av karbonater och accessoriskt förekommer magnetit, pyrit, klorit, apatit och gips. Magmatiska flytstrukturer är vanliga i proven.

Sammansättningen hos de kvartsförande porfyrerna i hängväggen är till stor del samma som hos gångporfyrerna. Kvarts förekommer i något högre grad i de kvartsförande porfyrerna och grundmassan är i de flesta fall röd till mörkgrå. Tydliga flytstrukturer förekommer även här och de två prov från malm – hängväggskontakt visar komplexa kontaktförhållanden.

Geokemidatan från LKAB:s databas som här använts som referensmaterial innehöll från början 21 838 analyser. Analyser med Fe_2O_3 -halter högre än 10 % har sedan exkluderats för att minimera provens påverkan av järnmalmen och kvar blir 17 688 analyser. Ytterligare har Hughes (1972) ”igneous spectrum” använts för att sålla bort analyser påverkade Na- och K-metasomatos, vilket slutligen lämnar kvar 4862 analyser som representerar möjligast opåverkade prov.

TAS klassifieringsdiagram (Le Maitre et al. 1989) för huvudelement med totala alkalier mot kisel visar att gångporfyrerna sträcker sig från intermediär till ryolitisk sammansättning överlappandes både häng- och liggväggsporfyrer. Diagram efter Pearce (1996) med immobila spårelement placerar däremot gångporfyrerna och hängväggsporfyrerna i det ryolitiska fältet medan liggvägsporfyrerna hamnar i andesitfältet. Diagram för aluminiumoxidmättnad plottar i huvudsak alla här behandlade bergarter på varandra som ”metaluminous” medan diagram Al_2O_3/TiO_2 vs Zr/Al_2O_3 efter Barrett et al. (2005), med mer immobila element, ger en separering av häng- och liggvägg med gångporfyrerna överlappande hängväggsporfyrerna. Tektoniskt diskrimineringsdiagram efter Gorton & Schandl (2000) visar en större spridning men analyserna koncentreras i fältet för en aktiv kontinentalgräns.

En U-Pb-åldersdatering gjordes på zirkon från prov F2121/1223. Provet är rikt på euhedrala till subhedrala zirkoner, 30-40 µm breda och 50-150 µm långa, med oscillerande zonering. Av 40 analyser är 26 konkordanta och ger en konkordiaålder på 1879,6 ± 4,2 Ma vilket representerar kristallisationsåldern för provet.

Diskussion

Fältobservationer av gångporfyrerna visar att dess porfyriska textur är mer eller mindre identisk med den hos hängväggsporfyrerna. Fenokristernas storlek, form, färg och fördelning tillsammans med grundmassans egenskaper varierar mellan olika prov men som tidigare noterat av Geijer (1919) och Sandberg (2018) är båda porfyrer i stora drag konsekvent lika. Även i mikroskopisk skala kan skillnader i varken textur eller mineralogi urskiljas.

Ett antal prov i denna studie innehåller biotit, vilket också nämns som en beståndsdel i gångporfyrer av Geijer (1910), men däremot har ingen biotit påträffats i prover från Sandberg (2018), som här använts som referensmaterial. Eftersom prover av både gångporfyrer och hängväggsporfyrer rika på biotit nästan helt och hållet saknar klinopyroxen och amfibol tyder det på att de ersatts av biotiten. Sandberg (2018) kommer till slutsatsen att gångporfyrerna innehåller mindre kvarts och mer klinopyroxen än de kvartsbärande porfyrerna. Detta stämmer överens med de gröna proven i denna studie, men inte de rödfärgade. Färgvariationerna hos

proven beror på mineralogiska skillnader i grundmassan. Klinopyroxen och amfibol är dominerande i grundmassan hos de prov som uppträder gröna till färgen medan de röda proven kan ha en finkornigare grundmassa där fältspat färgats av järnoxidinneslutningar.

Kontakter mellan gångporfyrer och malmen uppvisar både genomskärande skarpa kontakter och tecken på ’magma mingling’, med rundade enklaver av gångporfyr i malmen. Liknande relationer kan observeras mellan hängväggsporfyrerna och malmen, liksom enklaver av malm inuti hängväggen (Geijer 1968; Andersson 2013). Detta tyder på en samtidig existens av magmapulser av gångporfyr som av järnoxidmagma, som tidigare diskuterats av Geijer (1910, 1919, 1960) och Andersson (2013). Den sistnämnda tolkar även gångporfyrerna som tillförselkanaler till åtminstone en del av hängväggsvulkanismen.

Konkordiaåldern 1880±4 Ma, som erhållits i denna studie, anses representera kristallisationsåldern hos gångporfyrerna. Åldern faller inom ramarna för tidigare studieresultat av Kiirunavaaras malm och intilliggande sidoberg (Romer et al. 1994; Westhues et al. 2016; Billström et al. 2019). Överlappande kristallisationsåldrar i området tyder på nära i tid aktiva magmor.

Geokemiresultaten visar att gångporfyrerna liksom de andra silikatbergarterna i Kiirunavaara är kraftigt natriumomvandlade. Därav var den bearbetning av data som finns beskriven ovan nödvändig för att kunna jämföra bergarternas närmast möjliga ursprungssammansättning.

Resultat från denna studie och referensdata från LKAB:s databas på gångporfyrer samt kvartsbärande porfyrer visar att de är geokemiskt identiska och plottar över varandra i alla geokemidiagrammen. Syenitporfyrerna plottar i stort sett överlappande de tidigare nämnda porfyrerna i huvudelementdiagrammen, medan en avvikelse uppkommer i spårelementdiagrammen. Detta tyder på att spårelementen i högre grad kan användas för att undkomma den kraftiga alkaliomvandling som skett i silikatbergarterna.

Geokemidata från denna studie visar en uppdelning av gröna och röda prover i TAS-klassificeringsdiagrammet och IOCG-diskrimineringsdiagrammet. De gröna proverna faller även i stort sett utanför ”igneous spectrum” i Hughes (1972), vilket tyder på att de gröna proverna i större utsträckning utsatts av alkaliomvandlingen. Studier av Paolillo och Giapis (2021) och Lupoli et al. (2022) diskuterar en genomgripande Na-omvandling i Kiirunavaaras hängvägg, med en Na-Ca-omvandling närmast malmen följt av Ca-Fe-omvandling och sedan K-Fe-omvandling i de avlägsnare delarna. Även en möjlig senare kaliumomvandling där biotit ersatt aktinolit nämns av Lupoli et al. (2022). Gångporfyrprov i denna studie visar passande resultat med en påtaglig Na-omvandling och indikationer på Ca-Fe-omvandling. De röda proverna skulle representera en Na- Na-Ca-dominerad omvandling och de gröna tyder mer på en Ca-Fe-omvandling.

Största delen av Kiirunavaaras silikatbergarter, även inkluderat gångporfyrerna, faller inom det metaluminösa fältet, vilket tyder på metavulkaniska källor hos bergarterna snarare än metasedimentära. Tektoniska diskrimineringsdiagrammet av Schandl och Gorton (2002) visar en stor spridning av data men gångporfyrerna koncentreras i fältet för en aktiv kontinentalgräns och de andra sidobergarterna plottar lite bredare med en majoritet i fältet för aktiv kontinentalgräns och oceanisk öbåge-miljö. Detta stöder tidigare forskningsresultat och förslag på en kontinental 'arc'-miljö.

Slutsats

Resultaten bekräftar en genomgripande Na-omvandling för gångporfyrerna och Kiirunavaaras silikatbergarter generellt. Två karaktäristiska färgvariationer utmärker gångporfyrerna, en röd variant orsakad av järnoxidpigmentering i grundmassans finkorniga fältspater, och en grön variant orsakad av rikligt med de gröna silikaterna klinopyroxen och amfibol i grundmassan. En tredje mörk variant där de gröna silikaten ersatts av biotit förekommer också men är mindre uppenbar. De geokemiska skillnader hos de röda och gröna gångporfyrerna indikerar ursprung från två skilda magmapulser och/eller skillnader i metasomatisk omvandling. Den erhållna U-Pb konkordiaåldern 1880±4 Ma överlappar åldrarna hos de andra bergarterna i Kiirunavaaragruppen. Gångporfyrernas geokemi plottar identiskt med hängväggens kvartsförande porfyrer med vilka de också delar samma karaktäristiska mineralogi och textur.

Med tanke på ovanstående dras här slutsatsen att gångporfyrerna representerar magmor identiska till sammansättningen med hängväggsvulkanismen, till vilken de högst troligen representerar tillförselkanaler. Pulser av gångporfyrmagmor har intruderat i en aktiv kontinentalgräns tektonisk miljö vid avtagandet av malm- och liggväggsmagmatismen, vilket orsakat minglande strukturer med malmen men också genomskärande gångar.

REFERENCES

ALS (2023) Analystekniker. *https://www.alsglobal.se/Om-ALS-life-sciences/analystekniker [12.11.2023]*

Andersson, U.B. (2013) Coeval iron oxide and silicate magmas; structural evidence for immiscibility and mingling at Kiirunavaara, *in Mineral Deposit Research for a High-Tech World - 12th SGA Biennial Meeting 2013. Proceedings, Volume 4, p. 1635–1638*

Andersson, J.B.H., Bauer T.E., and Martinsson O. (2021) Structural Evolution of the Central Kiruna Area, Northern Norrbotten, Sweden: Implications on the Geologic Setting Generating Iron Oxide-Apatite and Epigenetic Iron and Copper Sulfides. *Economic geology and the Bulletin of the Society of Economic Geologists, Vol. 116, nr 8, p. 1981-2009*

Andersson, U.B., Klemo, L. and Liu, Y. (2019) Geologisk, petrografisk och geokemisk översikt av Per Geijer-mineraliseringarna och associerade bergarter. *LKAB Meddelande 2019-20081, 41 pp.*

Andersson, U.B. & Rutanen, H. (2016) Geological features in and around the Kiirunavaara ore body, northernmost Sweden, and some implications. *International Geological Congress, Cape Town, 2016- 08-27—09-04, Paper Nr. 2989.*

Andersson, U.B., Pihl, J., Bäckström, A., Fröjdö, S. & Eklund, O. (2024): Dyke porphyries in Kiirunavaara: feeders of the hanging wall volcanism. *36:e Nordiska geologiska vintermötet, Göteborg, 10-12/1 2024.*

Aspvik, J. (2000): Karta samt beskrivning över magnetitbreccia och omgivande bergarter på Kiirunavaaras topp. *Praktik i Petrologi/Geokemi 5p, Stockholms univ., 15 pp*

Aupers K. (2014) Gangue mineralogy and deportment of deleterious elements in the iron ore of the Kiirunavaara deposit, Sweden. *Master thesis, TU Bergakademie Freiberg, 151 p.*

Barrett, T.J., MacLean, W.H., and Årebäck, H. (2005) The Palaeoproterozoic Kristineberg VMS deposit, Skellefte district, northern Sweden. Part 2: chemostratigraphy and alteration. *Mineralium Deposita, DOI 10.1007/s00126-005-0001-2.*

Belousova E.A., Griffin W.L., O'Reilly S.Y. (2006) Zircon crystal morphology, trace element signatures and Hf isotope composition as a tool for petrogenetic modeling: examples from Eastern Australian granitoids. *J Petrol 47:329–353*

Berglund, J. & Andersson, U.B., (2013) Kinematic analysis of geological structures in Block 34, Kiirunavaara.. *LKAB Investigation 13-746, 48 pp + 2 Appendices, 29 pp.*

Berglund, J., Petersson, J. & Edland-Faber, M. (2010) Petrographic description of thin sections from Kiruna. *Vattenfall Power Consultant, Report, 2010-10-29, pp. 48 + Appendix.*

Bergman, S., Kubler, L., and Martinsson, O., (2001) Description of regional geological and geophysical maps of northern Norrbotten county (east of the Caledonian orogen). *Sveriges Geologiska Undersökning, Ba 56, 110 pp.*

Bergman, S., and Weihed, P., (2020) Archean (>2.6 Ga) and Paleoproterozoic (2.5–1.8 Ga), pre- and syn-orogenic magmatism, sedimentation and mineralization in the Norrbotten and Överkalix lithotectonic units, Svecokarelian orogeny: *Geological Society, London, Memoir 50, p. 27–82.*

Billström, K., Evins, P., Martinsson, O., Jeon, H., Weihed, P. (2019) Conflicting zircon vs. titanite U-Pb age systematics and the deposition of the host volcanic sequence to Kiruna-type

and IOCG deposits in northern Sweden, Fennoscandian shield. *Precambrian Research 321, 123-133.*

Björnell, T., Andersson, U.B., Eriksson, P., Faber, M. & Larsson, C.-F. (2015) Structural mapping and 3-D photographing, in and around block 34, levels 1079-1137, in the Kiirunavaara mine. *LKAB Investigation 15-820, 90 pp. + 3 Appendices, 34 pp.*

Chappell, B.W. & Stephens, W.E. (1988) Origin of infracrustal (I-type) granite magmas. *Transactions of the Royal Society of Edinburgh, Earth Sciences 79, 71-86.*

Ekström, M. & Ekström, T. (1997) Petrografisk beskrivning av sidoberget i Kiirunavaara. *Ekström Mineral AB, 21 pp.*

Frietsch, R. (1979) Petrology of the Kurravaara area Northeast of Kiruna Northern Sweden. *Sveriges Geologiska Undersökning C 760, 62 p.*

Frietsch, R. (1984) On the Magmatic Origin of the Iron Ores of the Kiruna Type – A reply. *Economic geology and the bulletin of the Society of Economic Geologists, Vol. 79, no 8, pp. 1949-1951*

Geijer, P. (1910a) Igneous rocks and iron ores of Kiirunavaara, Luossavaara and Tuollavaara. Scientific and Practical Researches in Lapland arranged by the Luossavaara-Kiirunavaara Aktiebolag, *Geology of the Kiruna district 2, Stockholm, 278 pp.*

Geijer, P. (1910b) Igneous rocks and iron ores of Kiirunavaara, Luossavaara and Tuolluvaara. *Economic Geology, Vol. 5, No.8, pp. 699–718.*

Geijer, P. (1919) Recent developments at Kiruna. *Geol. Surv. Sweden, C no. 288 22 pp.*

Geijer, P. (1931) The iron ores of the Kiruna type. *Geol. Surv. Sweden, C no. 367, 39 pp.*

Geijer, P. (1950) The Rektor ore body at Kiruna*., Geol. Surv. Sweden, ser. C no. 514, 18 pp.*

Geijer, P. (1960) The Kiruna iron ores - Sulphide and iron ores of Västerbotten and Lappland, northern Sweden. *Guide to Excursions Nos. A 27 and C 22.*

Geijer, P. (1968) Problemen kring malmbrottstycken i Kirunas hängväggsporfyr, *Geol. Surv. Sweden C 629, 34 pp.*

Gilg, H.A., & Andersson, U.B. (2020) Geology of deep clay alteration zones in the Kiirunavaara and other iron ore deposits, northern Norrbotten, Sweden. *LKAB Investigation 2020-0053, 30 pp.*

Gorton, M.P., and Schandl, E.S. (2000) From continents to island arcs: A geochemical index of tectonic setting for arc-related and within-plate felsic to intermediate volcanic rocks. *Canadian Mineralogist, v. 38, p. 1065–1073, https://doi.org/10.2113/gscanmin.38.5.1065*

Gray, W. (2016) Genesis of the Kiirunavaara nodular porphyry and Kiruna-type iron deposits: clues from titanite geothermometry and magnetite trace element composition. *Honours thesis, University of St. Andrews, UK, 54 p.*

Harley, S.L., & Kelly, N.M. (2007) Zircon Tiny but Timely. *Elements*, *vol. 3, No. 1, p. 13-18.*

Hilmo, J., Miles, J., and Bacquet, I. (2022) A preliminary comparison of the Per Geijer and Kiirunavaara apatite-iron oxide (AIO) deposits. *Geological Society of Sweden, Anniversary Meeting 2022, Thematic session 2, p. 132-133*

Hitzman, M.W., Oreskes, N. and Einaudi, M.T. (1992) Geological characteristics and tectonic setting of Proterozoic iron oxide (Cu-U-Au-REE) deposits. *Prec Res 58: 241-287.*

Hughes, C.J. (1972) Spilites, keratophyres, and the igneous spectrum. *Geological Magazine, vol. 109, pp. 513–527 doi:10.1017/S0016756800042795*

Huhma, H., Mänttäri, I., Peltonen, P., Kontinen, A., Halkoaho, T., Hanski, E., Hokkanen, T., Hölttä, P., Juopperi, H., Konnunaho, J., Layahe, Y., Luukkonen. E., Pietikäinen. K., Pulkkinen, A., Sorjonen-Ward, P., Vaasjoki, M. & Whitehouse, M. (2012) The age of the Archaean greenstone belts in Finland. *Geological Survey of Finland, Special Paper 54, 74−175, 69 figures, 1 table and 4 appendices.*

Ireland, T.R., and Williams. I.S. (2003) Considerations in zircon geochronology by SIMS, *Reviews in Mineralogy and Geochemistry*, *Chapter 8, vol. 53, p. 215-242.*

Le Maitre, R.W. (1989) A Classification of Igneous Rocks and Glossary of Terms. Recommendations of the IUGS Commission on the Systematics of Igneous Rocks. Oxford: Blackwell. Derived from work done in Le Bas, M. J., Le Maitre, R. W., Streckeisen, A. and Zanettin, B. (1986). A chemical classification of volcanic rocks based on the total alkali-silica diagram. *Journal of Petrology 27, 745-750.*

Lindgren, K. (2013). Punklasttestning av olika bergartstyper i Kiirunavaaras liggvägg. *Teknologie kandidatexamen Naturresursteknik, Luleå Tekniska Universitet, 102 pp.*

Lundberg, B., Smellie, J.A.T. (1979) Painirova and Mertainen iron ores: two deposits of the Kiruna Iron Ore type in northern Sweden: *Econ. Geology 74, 1131–1152.*

Lupoli, P., Lobo, L., Katai, O., Prata, R., Santana, C., Gerlach, L., Benedicto, C., Johansson, S., Friedländer M.-L., Martins M., and Biedzio, P. (2022) Proximal hydrothermal alteration assemblages in the Kiruna deposit – a preliminary petrographic study. *LITHOSPHERE 2022 Symposium, November 15-17, Turku.*

Löfstrand, G. (1891) Äro jernmalmerna och apatiten i Norrbotten lagerbildningar?, *Geologiska Föreningen i Stockholm Förhandlingar, 13:4, p. 335-372.*

Martinsson, O. & Erlandsson, M. (2009) Prospekteringsobjekt LKAB, ”Framtida järnmalmsfyndigheter i Malmfälten”. Fältarbete 2006-2008: objekt Lappmalmen. *Geovista GVR 09018, 68 sid. + Bil.*

Martinsson, O., and Hansson, K.-E., (2004) Apatite iron ores in the Kiruna area: *Society of Economic Geologists, Guidebook Series, v. 33, p. 173–175.*

Martinsson, O., (2004) Geology and metallogeny of the northern Norrbotten Fe-Cu-Au province. *SEG Guide Book Series 33, 131-148.*

Martinsson, O., Vaasjoki, M. & Persson, P.-O., (1999) U-Pb ages of Archaean to Palaeoproterozoic granitoids in the Torneträsk-Råstojaure area, northern Sweden. In: S. Bergman (ed.): Radiometric dating results 4. *Sveriges geologiska undersökning C 831, 70–90.*

Martinsson, O., Billström, K., Broman., C., Weihed, P., and Wanhainen, C., 2016, Metallogeny of the Northern Norrbotten ore province, northern Fennoscandian Shield with emphasis on IOCG and apatite-iron ore deposits: *Ore Geology Reviews, v. 78, p. 447–492.*

Martinsson, O. (1997) Tectonic setting and metallogeny of the Kiruna greenstones. *PhD thesis, Luleå University of Technology, Sweden.*

Montreuil, J.F, Corriveau, L. and Grunsky, E.C. (2013) Compositional data analysis of hydrothermal alteration in IOCG systems, Great Bear magmatic zone, Canada: to each alteration type its own geochemical signature. *Geochemistry: Exploration, Environment, Analysis, vol.13, p. 229-247*

Müller, W., M. Shelley, Miller, P., Broude, S. (2009) "Initial performance metrics of a new custom-designed ArF excimer LA-ICPMS system coupled to a two-volume laser-ablation cell." *Journal of Analytical Atomic Spectrometry, 24: 209-214*

Niiranen, K., (2006) The Deep Parts of the Kiirunavaara Apatite-magnetite Ore Body in Kiruna, Northern Sweden and the Impact of Future mining on the Township of Kiruna. *Proceedings, 6th International Mining Geology Conference, Darwin, AusIMM, p. 57-67.*

Nordstrand, J. & Andersson, U.B. (2013) Mineral chemistry of gangue minerals of the Kiirunavaara iron ore, recording a transition from magmatic to hydrothermal conditions. *12th SGA Biennial Meeting, Proceedings, Uppsala, Sweden 12-15/8. Geological Survey of Sweden, pp. 1663-1666.*

Nyström, J-O. (1985) Apatite iron ores of the Kiruna field, northern Sweden: magmatic textures and carbonatitic affinity. *GFF 107: 133-141.*

Nyström, J. O., Billström, K., Henríquez, F., Fallick, A. E., Naslund, H.R. (2008) Oxygen isotope composition of magnetite in iron ores of the Kiruna type in Chile and Sweden. *GFF 130(4), 177-188.*

Palm, P. (2015) Footwall porphyry nodules of the Kiirunavaara and Loussavaara apatiteiron ores: Mineralogy and mineral chemistry of magnetite, amphibole and mica (B.Sc thesis). *Department of Earth Sciences, University of Gothenburg. 49 pp.*

Paolillo, L. & Giapis, C. (2021) A preliminary assessment of hydrothermal alterations in the giant Kiruna IOA deposit, Kiruna, Sweden. *LITHOSPHERE 2021 Symposium, January 19-20. pp. 107-110.*

Parák, T. (1975a) The Origin of the Kiruna Iron Ores. *Sveriges geologiska undersökning C709. 209 pp.*

Parák, T. (1975b) Kiruna iron Oreas Are Not "Intrusive-Magmatic Ores of the Kiruna Type". *Economic Geology, Vol. 70, pp. 1242-1258.*

Parrish, R.R., and Noble, S.R. (2003) Zircon U-Th-Pb geochronology by isotope dilution-thermal ionization mass spectrometry (ID-TIMS). *Reviews in Mineralogy and Geochemistry, Chapter 7. vol. 53, p. 183-214.*

Patchett, J. & Kouvo, O. (1986) Origin of continental crust of 1.9- 1.7 Ga age: Nd isotopes and U-Pb zircon ages in the Svecokarelian terrain of south Finland. *Contributions to Mineralogy and Petrology 92, 1-12.*

Pearce, J.A. (1982) Trace Element Characteristics of Lavas from Destructive Plate Boundaries. *In: Thorpe, R.S., Ed., Andesites: Orogenic Andesites and Related Rocks, John Wiley and Sons, 252-548.*

Pearce, J.A. (1983) Role of the Sub-Continental Lithosphere in Magma Genesis at Active Continental Margins. *In: Hawkesworth, C.J. and Norry, M.J., Eds., Continental Basalts and Mantle Xenoliths, Shiva Cheshire, UK, 230-249.*

Pearce, J.A. (1996) Volcanic Rocks Modified. Modified after Winchester and Floyd, (1977). Log Nb/Y vs Log Zr/Ti. Used as immobile element proxy for the TAS diagram. A user's guide to basalt discrimination diagrams. *In: Wyman, D. A. (ed.) Trace Element Geochemistry of*

Volcanic Rocks: Applications for Massive Sulphide Exploration. Geological Association of Canada, Short Course Notes 12, 79 to 113.

Peters, S.T.M., Feng, D., Troll, V.R., Pack, A., Andersson, U.B., Tornos, F., Lehmann, B., di Rocco, T. (2022) Triple oxygen isotope compositions of iron oxide-apatite deposits – a window into ore formation processes and the ancient atmosphere. *Deutsche Mineralogische Gesellschaft (DMG) 100th Annual Conference, GeoMinKöln, Cologne, Sept. 11-15th. Book of Abstracts, p. 301.*

Romer, R.L., Martinsson, O., and Perdahl, J.-A. (1994) Geochronology of the Kiruna iron ores and hydrothermal alterations. *Economic Geology 89, 1249–1261.*

Sandberg, H. (2018) A petrological investigation of the host rocks for the Kuj-Kiirunavaara ore*. Independent Project at the Dept. of EarthSciences 2018:2, 100 p.*

Sarlus, Z., Andersson, U.B., Bauer, T.E., Wanhainen, C., Martinsson, O., Nordin, R., Andersson, J.B. (2018) Timing of plutonism in the Gällivare area: implications for Proterozoic crustal development in the northern Norrbotten ore district, Sweden. *Geological Magazine 155(6), 1351-1376.*

Sarlus, Z., Andersson, U.B., Martinsson, O., Bauer, T.E., Wanhainen, C., Andersson, J.B., Whitehouse, M.J. (2020) Timing and origin of the host rocks to the Malmberget iron oxide-apatite deposit, Sweden. *Precambrian Research 342, 105652, 19 pp.*

Scaillet, B., Holtz, F. & Pichavant, M. (2016) Expermiental constraints on the formation of silicic magmas. *Elements 12: 109-114.*

Schandl, E.S. & Gorton, M.P. (2002) Application of high field strength elements to discriminate tectonic settings in VMS environments. *Economic Geology, 97: 629-642.*

Scherer, E.E., Whitehouse, M.J., and Münker, C. (2007) Zircon as a monitor of crustalgrowth. *Elements, vol. 3 No. 1, p. 19-24.*

Smith, M.P., Storey, C.D., Jeffries, T.E., and Ryan, C. (2009) In situ U-Pb and trace element analysis of accessory minerals in the Kiruna District, Norrbotten, Sweden: New constraints on the timing and origin of mineralization. *J. Petrol. 50: 2063-2091.*

Troll, V.R., Weis, F.A., Jonsson, E., Andersson, U.B., Majidi, S.A., Högdahl, K., Harris C., Millet, M.-A., Chinnasamy, S.S., Koojiman, E., Nilsson, K.P. (2019) Global Fe–O isotope correlation reveals magmatic origin of Kiruna-type apatite-iron-oxide ores. *Nature Communications 10(1), 1712, 12 pp + Suppl..*

Van Achterbergh, E., Ryan C., Jackson, S., and Griffin W., (2001) Data reduction software for LA-ICP-MS, in: Laser-Ablation ICPMS in the Earth Sciences – Principles and applications, *Mineralogical Association of Canada short course series, 29, St John, Newfoundland, Sylverster P. Ed., 239-243.*

Westhues, A., Hanchar, J.M., Whitehouse, M.J., and Martinsson, O. (2016) New constraints on the timing of host-rock emplacement, hydrothermal alteration, and iron oxide-apatite mineralization in the Kiruna district, Norrbotten, Sweden: *Economic Geology, v. 111, p. 1595–1618.*

Westhues, A., Hanchar, J.M, Voisey, C.R., Whitehouse, M.J., Rossman, G.R., and Wirth, R. (2017) Tracing the fluid evolution of the Kiruna iron oxide apatite deposits using zircon, monazite, and whole rock trace elements and isotopic studies: *Chemical Geology, v. 466, p. 303–322.*

Witschard, F., (1984) The geological and tectonic evolution of the Precambrian of northern Sweden, a case for basement reactivation? *Precambrian Research, v. 23, p. 273–315.*

APPENDIX I

Sampling locations:

Visitor´s mine, level 540

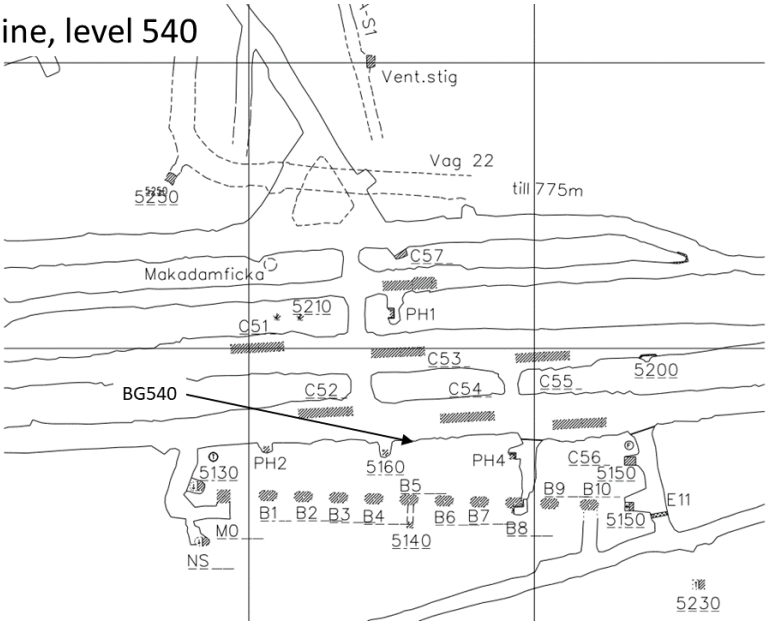

Block 8, level 1108

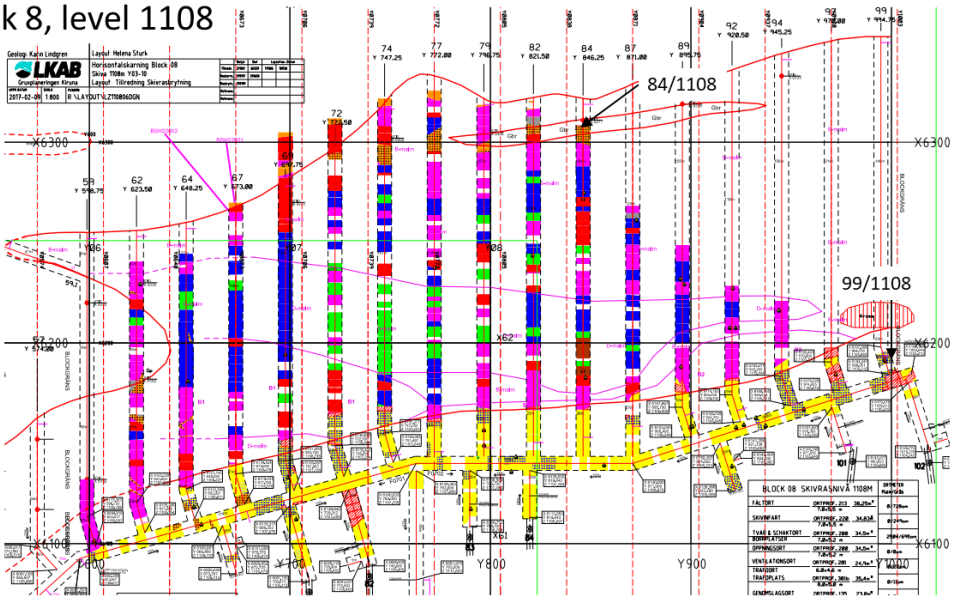

Block 12, level 1108

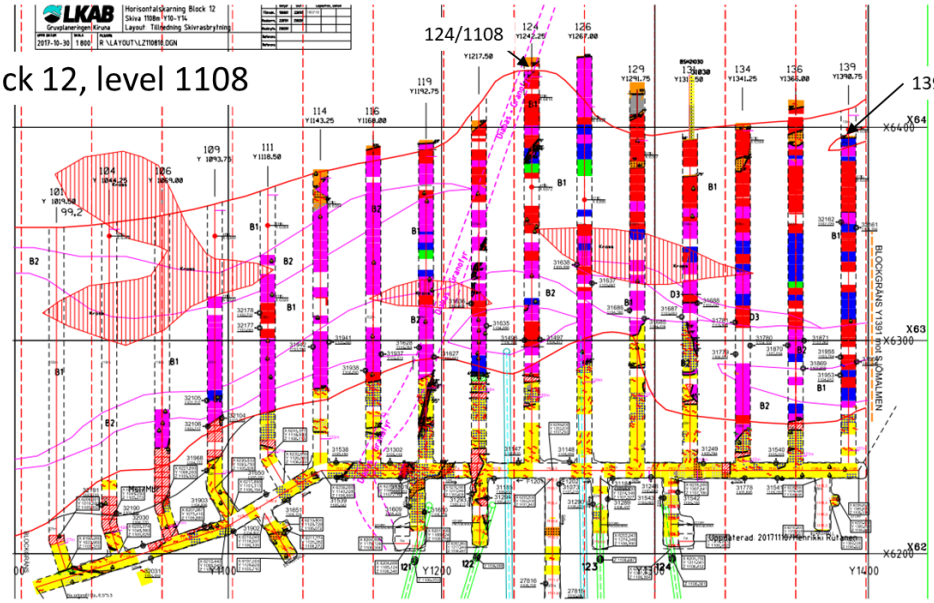

Block 12, level 1137

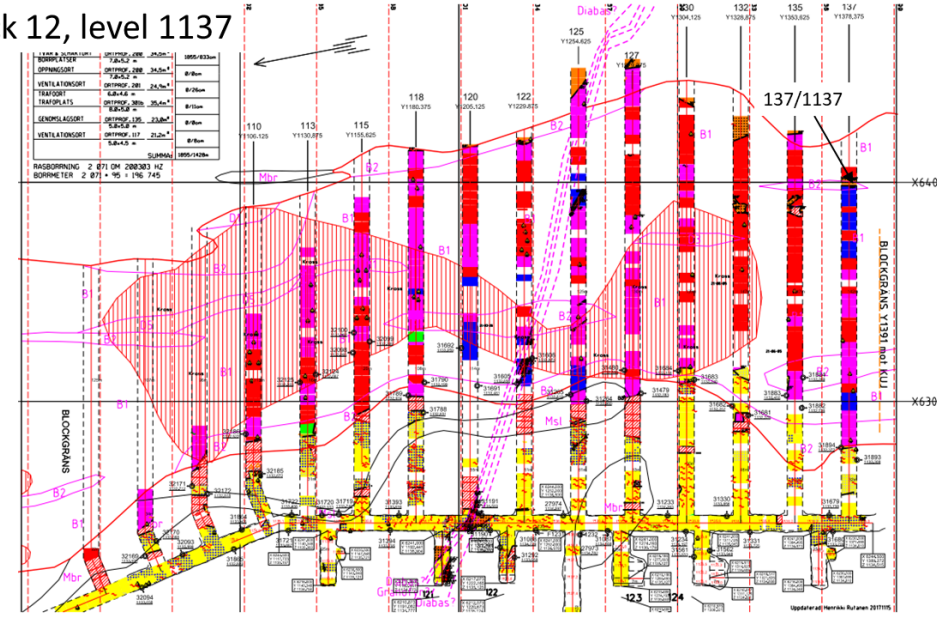

Block 15, level 1165

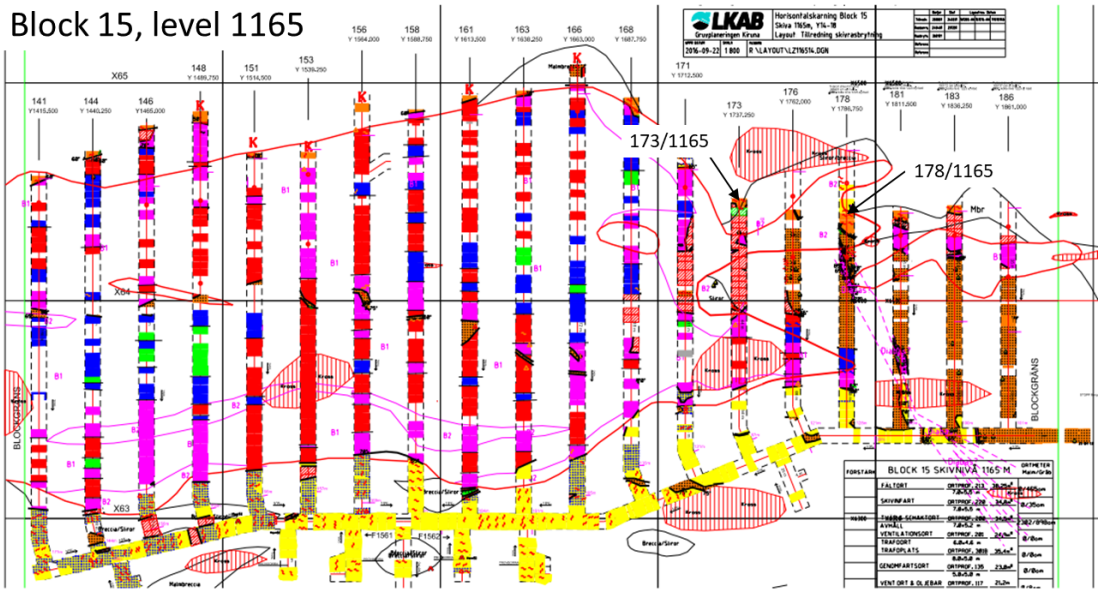

Block 22, level 1079

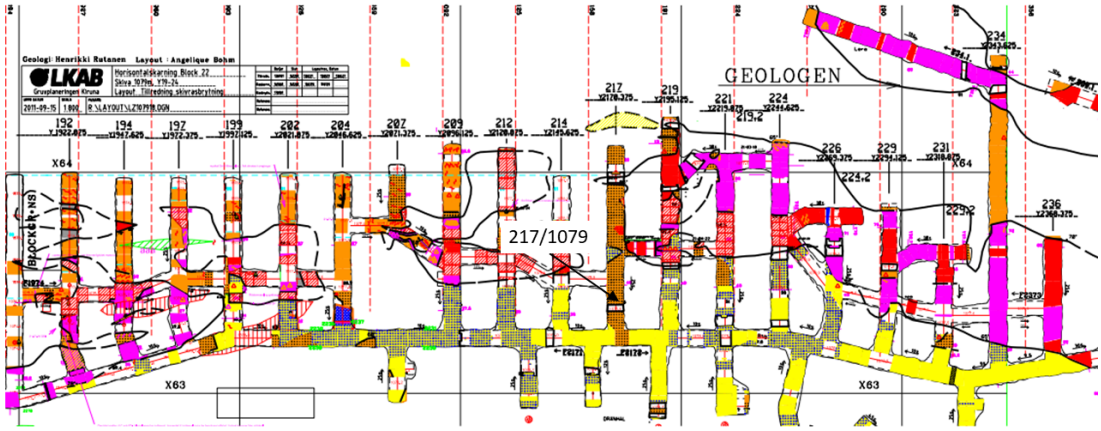

Block 22, level 1108

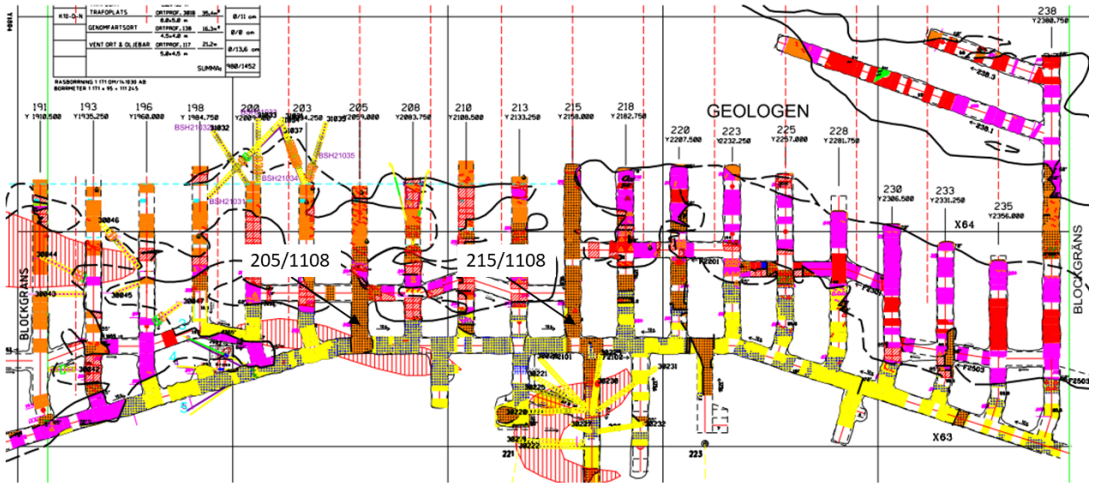

Block 22, level 1137

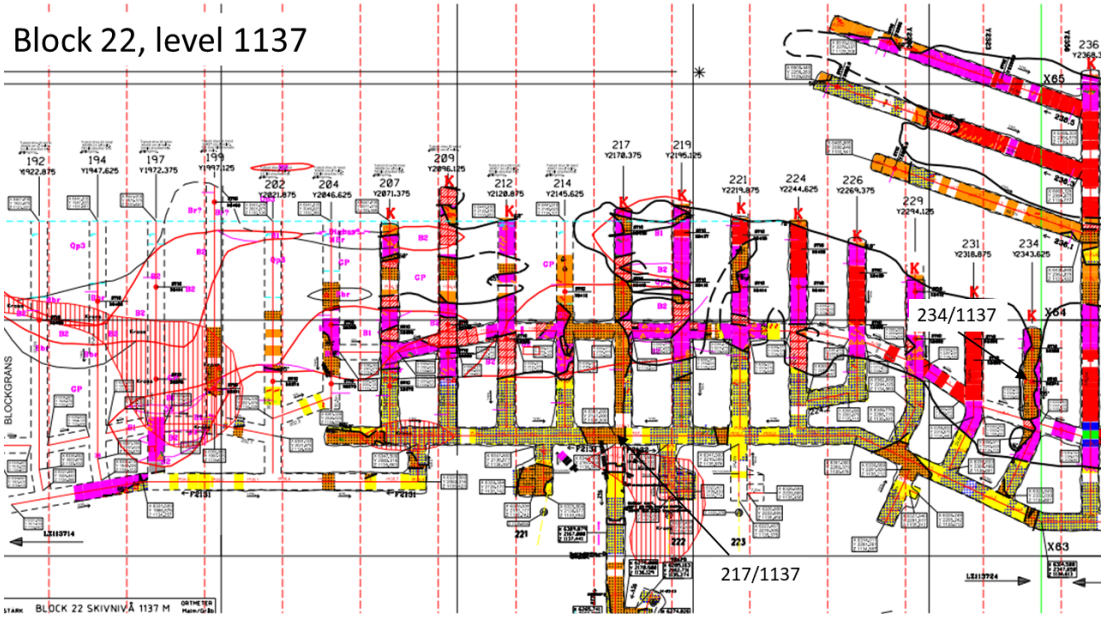

Block 22, level 1223

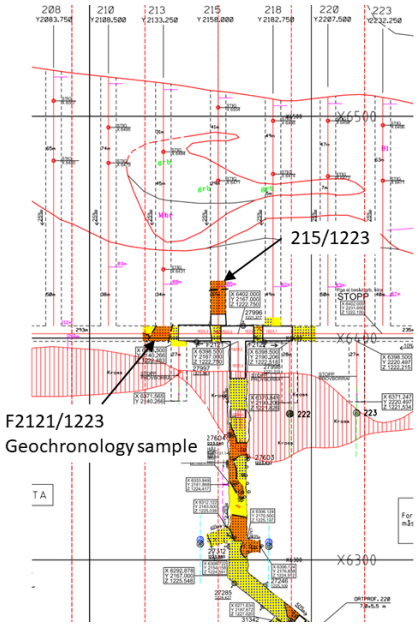

Block 30, level 1194

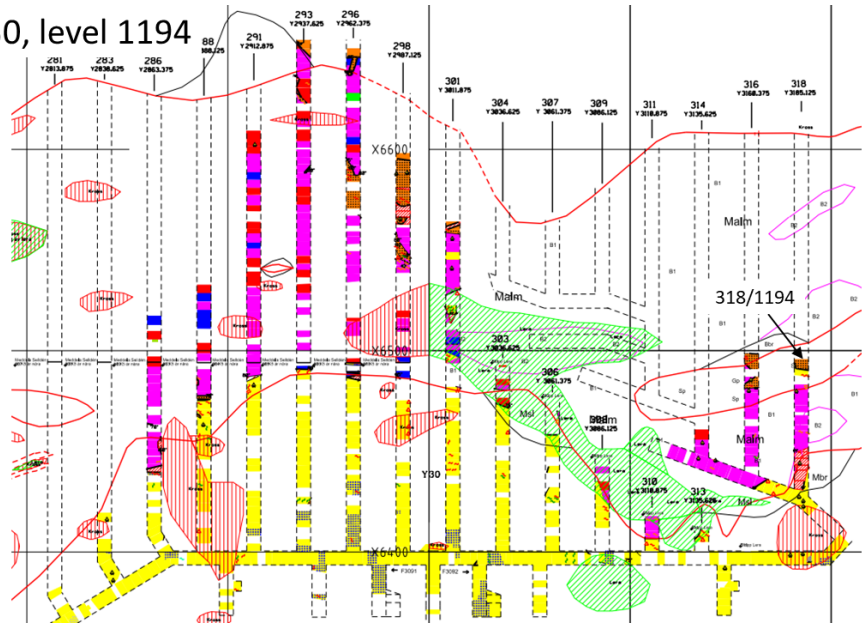

Block 34, level 1194

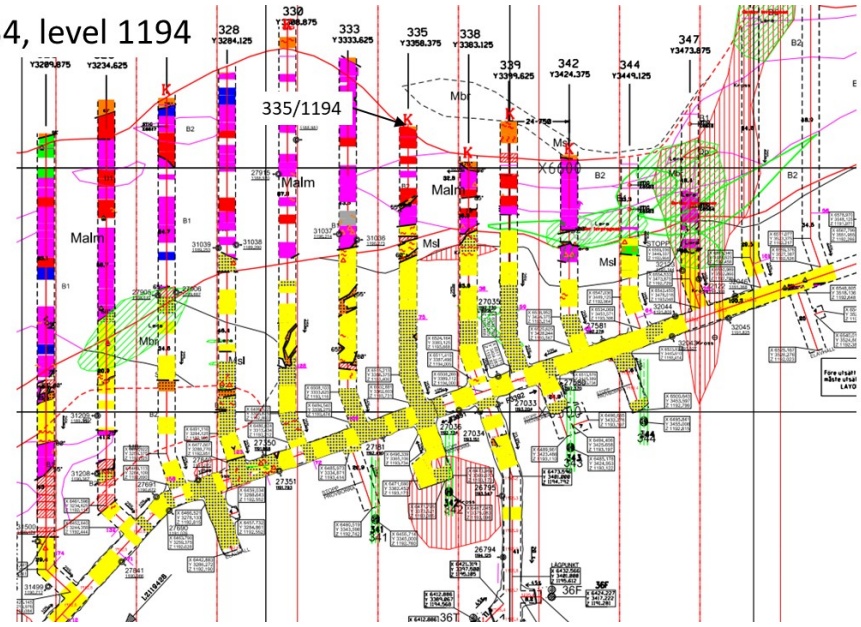

TG 34, level 1338

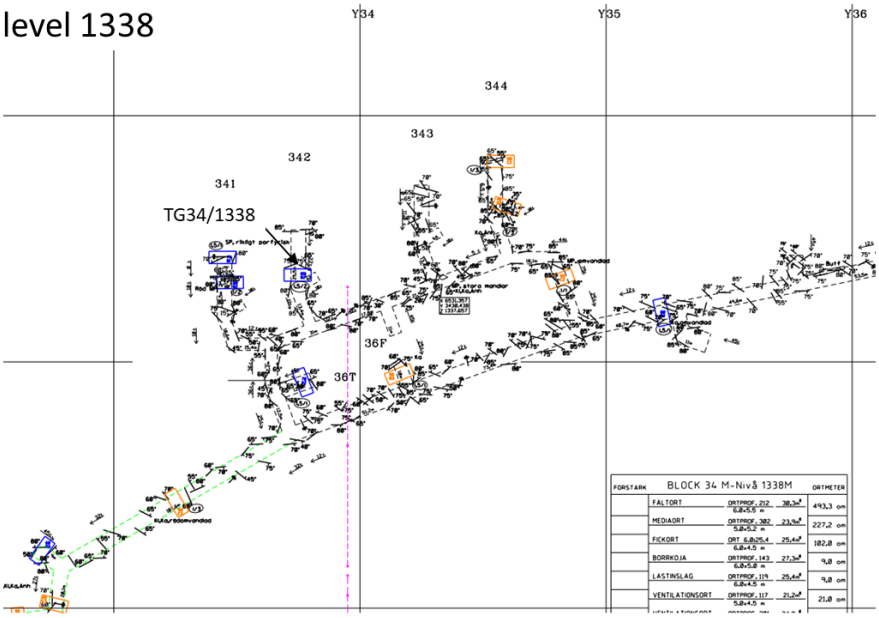

APPENDIX II

Geochemical data analysis results:

	ME-ICP06	ME-ICP06	ME-ICP06	ME-ICP06	ME-ICP06	ME-ICP06	ME-ICP06	ME-ICP06	ME-ICP06	ME-ICP06	ME-ICP06	ME-ICP06	ME-ICP06	TOT-ICP06
SAMPLE	SiO2	Al2O3	Fe2O3	CaO	MgO	Na2O	K2O	Cr2O3	TiO2	MnO	P2O5	SrO	BaO	Total
DESCRIPTION	%	%	%	%	%	%	%	%	%	%	%	%	%	%
217/1137	70.7	14.8	0.99	1.72	0.81	6.9	2.79	<0.002	0.43	0.02	<0.01	<0.01	0.05	99.72
217/1079	68.8	14.5	1.12	2.32	1.04	6.89	2.38	0.006	0.43	0.02	<0.01	<0.01	0.08	98.56
99/1108 A	57.4	11.85	3.53	8.65	4.8	4.19	4.23	0.002	0.4	0.09	0.01	<0.01	0.06	97.77
BG540	63.3	13.6	3.03	7.34	4.71	8.04	0.14	<0.002	0.34	0.09	0.01	<0.01	0.02	101.1
234/1137	60.2	12.8	4.37	4.33	5.38	6.37	1.58	<0.002	0.28	0.1	<0.01	<0.01	0.03	97.78
TG34/1338 G	61.5	11.7	4.21	7.49	5.88	4.44	3.86	<0.002	0.08	0.14	<0.01	<0.01	0.06	99.96
TG34/1338 R	70.1	13.95	1.34	3.03	1.25	5.27	4.53	<0.002	0.32	0.05	0.02	<0.01	0.09	101.55
F2121/1223	71.9	14.35	1.1	1.7	0.76	6.51	2.94	<0.002	0.33	0.02	0.01	<0.01	0.06	100.72
84/1108	68.7	13.05	2.34	1.93	2.54	6.62	1.32	<0.002	0.03	0.01	<0.01	<0.01	0.01	99.45
318/1194 A	62.6	13.2	3.12	7.16	4.55	5.56	3.54	<0.002	0.44	0.13	0.05	<0.01	0.05	100.68
137/1137 A	69.7	14.25	1.5	1.67	1.04	6.25	3.08	0.003	0.33	0.02	0.01	<0.01	0.06	99.04
139/1108 A	69.5	14.1	1.68	1.84	0.73	4.99	4.97	<0.002	0.32	0.02	0.01	<0.01	0.09	98.89
215/1108	67.6	14.05	1.96	2.34	2.54	6.87	2.09	<0.002	0.41	0.04	<0.01	<0.01	0.08	98.58
215/1223	62.1	14.05	2.94	6.38	3.67	6.78	2.34	<0.002	0.69	0.09	0.02	<0.01	0.05	99.73
205/1108 G	63.3	13.55	2.92	6.59	4.24	6.76	2.26	<0.002	0.34	0.09	<0.01	<0.01	0.03	101.99
205/1108 R	69.1	14.8	1.66	2.34	1.24	6.76	3.02	0.008	0.68	0.04	<0.01	<0.01	0.06	100.16
335/1194	67.1	14.2	2.45	2.32	2.15	6.02	3.43	<0.002	0.33	0.05	0.01	<0.01	0.09	98.57
124/1108	68.9	12.9	3.37	0.94	1.96	4.84	3.74	<0.002	0.15	0.03	0.01	<0.01	0.05	98.46

	ME-MS81	ME-MS81	ME-MS81	ME-MS81	ME-MS81	ME-MS81	ME-MS81	ME-MS81	ME-MS81	ME-MS81	ME-MS81	ME-MS81	ME-MS81	ME-MS81	ME-MS81
SAMPLE	Ba	Ce	Cr	Cs	Dy	Er	Eu	Ga	Gd	Hf	Ho	La	Lu	Nb	Nd
DESCRIPTION	ppm	ppm	ppm	ppm	ppm	ppm	ppm	ppm	ppm	ppm	ppm	ppm	ppm	ppm	ppm
217/1137	432	98.8	18	0.05	9.63	5.3	2.77	22.8	10.6	10.8	1.86	27.9	0.72	13.9	64.1
217/1079	679	110.5	57	0.02	9.75	5.84	2.71	21.7	11.15	11.1	2.06	34.1	0.74	17.2	68.3
99/1108 A	543	98.7	7	0.03	12.45	8.33	2.28	16.4	11.95	8.83	2.7	37.1	1.42	13.4	56.1
BG540	132.5	68.9	12	<0.01	8.76	5.33	1.66	20.2	8.4	10.75	1.9	22	0.98	9.44	43.4
234/1137	294	69.2	7	0.62	9.23	6.1	1.83	21.7	9.36	10.25	2.07	23	1.16	9.19	43.6
TG34/1338 G	554	37.3	6	0.01	6.63	4.33	1.1	19.6	6.09	10.5	1.42	14.9	0.81	1.1	25.4
TG34/1338 R	795	75.4	29	0.07	8.52	5	1.86	21.2	8.8	10.75	1.73	21.5	0.7	14.95	50.2
F2121/1223	548	67.9	15	0.05	9.15	4.89	2.06	23	9.09	11.85	1.79	19.2	0.77	13.6	48.6
84/1108	81.3	19	17	0.63	2.68	2.05	0.44	19.8	2.23	12	0.58	12	0.47	1.12	7.6
318/1194 A	464	87.6	14	0.07	11.5	6.98	2.21	20.9	10.7	9.24	2.59	33.8	1.17	13.9	51.9
137/1137 A	483	69.1	27	0.08	4.67	2.73	1.48	21.8	4.49	11.3	0.9	30.6	0.55	8.94	31.3
139/1108 A	738	55.1	14	0.01	4.19	2.55	1.34	20.7	3.89	11.25	0.98	24.2	0.59	7.63	23.1
215/1108	710	105	48	0.06	11.8	6.36	2.75	23.6	12.6	10.4	2.43	31	1.06	17.95	74.1
215/1223	464	157	15	0.02	15.95	9.07	4.19	22.1	19.1	8.64	3.39	46.2	1.24	18.2	108.5
205/1108 G	258	96.2	24	0.05	11.7	6.77	2.41	21.8	12.45	9.88	2.47	28.5	1.08	11.4	65.6
205/1108 R	514	147	32	0.04	15.65	8.49	3.78	22.9	17.25	11.25	3.13	39.2	1.09	24.7	104
335/1194	812	57.1	8	0.02	4.76	3	1.58	22.4	4.61	10.95	1.04	25.2	0.71	5.44	25.4
124/1108	417	23.5	8	0.39	2.82	1.92	0.58	20.4	2.45	12.75	0.65	12.5	0.47	2.7	10.5

	ME-MS81	ME-MS81	ME-MS81	ME-MS81	ME-MS81	ME-MS81	ME-MS81	ME-MS81	ME-MS81	ME-MS81	ME-MS81	ME-MS81	ME-MS81	ME-MS81	ME-MS81
SAMPLE	Pr	Rb	Sm	Sn	Sr	Ta	Tb	Th	Tm	U	V	W	Y	Yb	Zr
DESCRIPTION	ppm	ppm	ppm	ppm	ppm	ppm	ppm	ppm	ppm	ppm	ppm	ppm	ppm	ppm	ppm
217/1137	15.4	45.8	12.5	2.3	60.7	0.8	1.53	11.1	0.76	1.54	12	160	52.8	4.74	455
217/1079	16.3	35.3	13.5	1.7	96	0.5	1.72	10.85	0.89	1.99	14	158	52.6	5.37	450
99/1108 A	13.05	34.5	12.35	1.9	128.5	<0.1	1.91	10.75	1.24	3.61	52	91.6	72.2	8.4	361
BG540	10.55	2.5	8.71	1.9	59.4	0.6	1.34	5.18	0.88	1.26	56	116	50.8	5.56	433
234/1137	10.2	49.3	10.4	3.4	53.5	0.6	1.51	6.55	0.93	1.4	40	76.6	57.2	6.62	434
TG34/1338 G	5.71	34.5	5.96	1.4	35	0.2	0.98	4.85	0.73	1.2	49	103.5	40.9	4.91	452
TG34/1338 R	11.8	68.5	10.75	1.1	92.4	0.2	1.38	5.87	0.75	1.48	15	168.5	46.2	4.77	451
F2121/1223	10.95	38.8	10.55	1.6	68.9	0.9	1.47	7.74	0.74	1.44	10	197.5	46.3	4.84	480
84/1108	1.95	49.7	1.88	0.8	74.6	<0.1	0.38	2.92	0.28	1.53	9	267	16.4	2.38	472
318/1194 A	12.35	55.1	11.4	3.3	51.1	0.9	1.72	9.2	1.06	1.78	52	80.2	67.5	7.7	386
137/1137 A	8.05	37.8	4.71	1.6	52.6	0.6	0.66	5.81	0.42	2.46	10	217	27.1	3.18	468
139/1108 A	6.49	58.8	4.39	1.9	59.1	0.8	0.65	7.14	0.4	2.77	8	501	26.1	3.31	474
215/1108	16.55	33.1	15.55	2.5	71.2	0.9	1.83	8.16	0.97	2.3	25	262	65.6	6.73	447
215/1223	23.8	33.9	21.7	2.2	94.6	0.2	2.83	9.05	1.28	2.33	50	137	86.3	8.31	371
205/1108 G	15.05	32.6	13.6	1.8	46.1	1.4	1.81	8.78	1.05	3	45	78.6	68.1	7.45	422
205/1108 R	24	46	21.5	3.1	61.2	0.8	2.62	9.42	1.25	1.63	20	162	83.2	7.59	478
335/1194	6.74	41.3	4.74	2.1	60	0.6	0.77	9.28	0.54	1.96	24	127	30.3	3.79	472
124/1108	2.6	44.1	2.21	1.1	44.7	0.4	0.39	3.2	0.32	1.82	8	186	18	2.52	532

APPENDIX III

U-Pb analysis results

Analysis spot no.	Pb	Th	U	207Pb/206Pb	1s	207Pb/235U	1s	206Pb/238U	1s	% Concordance	207Pb/206Pb	1s	207Pb/235U	1s	206Pb/238U	1s
											Ma	Ma	Ma	Ma	Ma	Ma
F2121-1223_44a	44	151	138	0.1126	0.0006	3.804	0.080	0.245	0.005	77	1842	10	1594	17	1413	26
F2121-1223_162	65	150	153	0.1157	0.0008	5.080	0.108	0.318	0.006	94	1891	12	1833	18	1782	32
F2121-1223_52	26	44	66	0.1142	0.0008	5.036	0.108	0.320	0.007	96	1867	12	1825	18	1789	32
F2121-1223_114	30	40	72	0.1173	0.0014	5.367	0.124	0.332	0.007	96	1916	21	1880	20	1847	33
F2121-1223_76	14	20	36	0.1107	0.0009	4.780	0.103	0.313	0.006	97	1812	14	1781	18	1756	31
F2121-1223_01	46	39	121	0.1118	0.0007	4.979	0.106	0.323	0.007	99	1829	11	1816	18	1804	32
F2121-1223_122	23	29	60	0.1124	0.0018	5.050	0.128	0.326	0.007	99	1838	28	1828	21	1818	34
F2121-1223_04b	33	51	81	0.1134	0.0006	5.156	0.108	0.330	0.007	99	1854	10	1845	18	1838	32
F2121-1223_119b	36	44	87	0.1135	0.0010	5.348	0.117	0.342	0.007	102	1857	15	1877	19	1895	34
F2121-1223_31	36	77	83	0.1139	0.0006	5.285	0.111	0.337	0.007	100	1863	10	1866	18	1870	33
F2121-1223_80	43	76	99	0.1140	0.0007	5.439	0.115	0.346	0.007	103	1864	10	1891	18	1916	34
F2121-1223_39	46	80	105	0.1141	0.0006	5.492	0.115	0.349	0.007	103	1866	9	1899	18	1930	34
F2121-1223_04a	97	206	209	0.1141	0.0005	5.296	0.110	0.337	0.007	100	1866	9	1868	18	1870	33

Analysis spot no.	Pb	Th	U	207Pb/206Pb	1s	207Pb/235U	1s	206Pb/238U	1s	% Concordance	207Pb/206Pb	1s	207Pb/235U	1s	206Pb/238U	1s
											Ma	Ma	Ma	Ma	Ma	Ma
F2121-1223_44b	47	84	113	0.1143	0.0006	5.305	0.111	0.337	0.007	100	1868	9	1870	18	1871	33
F2121-1223_95a	29	63	67	0.1143	0.0008	5.277	0.113	0.335	0.007	100	1869	13	1865	18	1862	33
F2121-1223_71	27	50	63	0.1143	0.0007	5.336	0.113	0.338	0.007	101	1870	11	1875	18	1879	33
F2121-1223_95b	27	39	65	0.1145	0.0007	5.383	0.114	0.341	0.007	101	1872	12	1882	18	1891	33
F2121-1223_06	37	57	89	0.1147	0.0006	5.355	0.112	0.339	0.007	100	1876	10	1878	18	1880	33
F2121-1223_93	54	107	122	0.1149	0.0007	5.428	0.114	0.343	0.007	101	1879	11	1889	18	1899	33
F2121-1223_160	41	69	97	0.1150	0.0008	5.424	0.116	0.342	0.007	101	1879	12	1889	18	1897	33
F2121-1223_13b	26	39	62	0.1150	0.0007	5.469	0.115	0.345	0.007	102	1880	11	1896	18	1910	34
F2121-1223_148B	30	39	70	0.1155	0.0008	5.608	0.120	0.352	0.007	103	1888	13	1917	18	1944	34
F2121-1223_85	55	93	129	0.1157	0.0007	5.404	0.114	0.339	0.007	99	1891	11	1885	18	1881	33
F2121-1223_115	43	74	102	0.1157	0.0008	5.271	0.112	0.330	0.007	97	1892	12	1864	18	1840	33
F2121-1223_159	26	29	63	0.1158	0.0008	5.497	0.118	0.344	0.007	101	1893	13	1900	18	1907	34
F2121-1223_57	20	29	47	0.1159	0.0008	5.452	0.116	0.341	0.007	100	1894	12	1893	18	1892	33

Analysis spot no.	Pb	Th	U	207Pb/206Pb	1s	207Pb/235U	1s	206Pb/238U	1s	% Concordance	207Pb/206Pb	1s	207Pb/235U	1s	206Pb/238U	1s
											Ma	Ma	Ma	Ma	Ma	Ma
F2121-1223_139	30	40	67	0.1160	0.0009	5.586	0.121	0.349	0.007	102	1895	14	1914	19	1932	34
F2121-1223_81	34	56	80	0.1162	0.0008	5.316	0.114	0.332	0.007	97	1898	12	1871	18	1848	33
F2121-1223_13a	16	22	40	0.1163	0.0008	5.380	0.115	0.336	0.007	98	1900	12	1882	18	1865	33
F2121-1223_111	72	114	166	0.1166	0.0008	5.512	0.117	0.343	0.007	100	1905	12	1902	18	1900	33
F2121-1223_23	25	35	60	0.1166	0.0007	5.433	0.115	0.338	0.007	98	1905	11	1890	18	1876	33
F2121-1223_106	39	56	91	0.1167	0.0015	5.531	0.132	0.344	0.007	100	1907	23	1905	20	1904	34
F2121-1223_127	41	54	99	0.1172	0.0012	5.416	0.122	0.335	0.007	97	1913	18	1887	19	1864	33
F2121-1223_24	33	46	76	0.1179	0.0007	5.730	0.120	0.352	0.007	101	1925	10	1936	18	1946	34
F2121-1223_53	65	150	133	0.1157	0.0007	5.680	0.120	0.356	0.007	104	1891	11	1928	18	1963	34
F2121-1223_47	25	31	59	0.1149	0.0007	5.623	0.119	0.355	0.007	104	1878	11	1920	18	1958	34
F2121-1223_50	40	60	90	0.1158	0.0007	5.723	0.120	0.358	0.007	104	1893	10	1935	18	1974	35
F2121-1223_119a	52	82	126	0.1048	0.0010	4.722	0.106	0.327	0.007	107	1711	18	1771	19	1822	33
F2121-1223_148A	67	134	137	0.1149	0.0007	5.856	0.124	0.369	0.008	108	1879	12	1955	18	2027	35
F2121-1223_99	37	57	71	0.1072	0.0019	5.600	0.147	0.379	0.008	118	1753	32	1916	22	2071	38